Journal of Colloid and Interface Science 708 (2026) 139770

Contents lists available at ScienceDirect

Journal of Colloid And Interface Science

journal homepage: www.elsevier.com/locate/jcis

Stimuli-responsive microgels cross-linked through supramolecular interactions of peptides

Nadja A. Wolter [a,b], Gurudas Chakraborty [b], Hannah Küttner [a,b], Andreas Herrmann [a,b], Andrij Pich [a,b,c,*]

[a] Institute of Technical and Macromolecular Chemistry RWTH Aachen University, Worringerweg 2 52074, Aachen, Germany
[b] DWI – Leibniz Institute for Interactive Materials, Forckenbeckstraße 50 52074, Aachen, Germany
[c] Aachen-Maastricht Institute for Biobased Materials (AMIBM), Brightlands Chemelot Campus Urmonderbaan 22 6167, RD, Geleen, the Netherlands

HIGHLIGHTS

- Fabrication of PVCL-based microgels via noncovalent interactions of aromatic dipeptides
- Spectroscopic investigation of hydrogen bonding and π-π stacking-driven crosslinking
- Solvent-induced degradation of physical crosslinking
- Concentration-controlled morphology

GRAPHICAL ABSTRACT

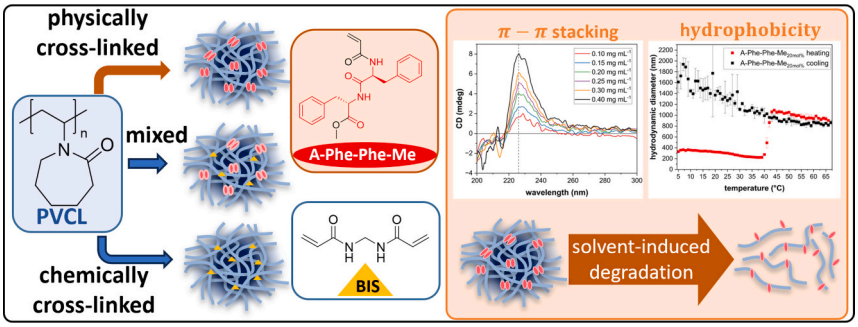

ARTICLE INFO

Keywords:
Self-assembly
Peptides
Supramolecular cross-links
Thermoresponsive microgels
Colloids

ABSTRACT

Stimuli-responsive microgels are colloidal polymer networks and the nature of the cross-links governs their ability to undergo reversible structural and topological changes in response to environmental stimuli such as temperature, pH, light, ionic strength, and mechanical force. Herein, we exploit the supramolecular interactions of the aromatic *L*-phenylalanyl-*L*-phenylalanine (Phe-Phe) dipeptide motif as a supramolecular cross-linker to fabricate poly-*N*-vinylcaprolactam (PVCL)-based thermoresponsive microgels. In the present work, we synthesize a series of microgels with variable content of Phe-Phe cross-links and quantify their amount (0.3–37 mol%) by nuclear magnetic resonance (^{1}H NMR) spectroscopy. We demonstrate that Phe-Phe cross-links retain the integrity and colloidal stability of microgels in aqueous solutions. Circular dichroism (CD) spectroscopy is employed to investigate aromatic π-π stacking of Phe moieties, confirming the formation of supramolecular cross-links. An increase in the Phe-Phe content or a decrease in microgel size induces temperature-dependent aggregation, which can be leveraged for the preparation of condition-guided microgel assemblies. Furthermore, we investigate solvent-induced degradation of physical cross-linking and dipeptide concentration-controlled morphological changes in the obtained microgels.

* Corresponding author.
E-mail address: pich@dwi.rwth-aachen.de (A. Pich).

https://doi.org/10.1016/j.jcis.2025.139770
Received 8 September 2025; Received in revised form 22 December 2025; Accepted 23 December 2025
Available online 24 December 2025

1. Introduction

Self-assembly is an essential process that makes life possible as it plays an important role in many biological processes, such as in the formation of deoxyribonucleic acid double helix or the formation of amyloid fibrils that play essential roles in various neurological diseases. Inspired by these processes found in biological systems, molecular self-assembly has been the subject of extensive research to construct biological as well as synthetic building blocks with hierarchical structures and tailored properties [1–3]. Molecular self-assembly, the spontaneous formation of well-defined ordered structures, relies on non-covalent interactions such as hydrogen bonding, electrostatic interactions, or aromatic stacking [3]. Targeted self-assembly, combined with responsive features and biocompatibility, are essential factors in designing tailored systems for biomedical applications. These systems rely on functional materials, with functional polymers being optimal candidates to meet these requirements [4].

Microgels are colloidal networks designed from cross-linked functional polymers, with a diameter between 0.1 and 100 μm [5,6]. Their stimuli-responsive behavior toward external stimuli, such as temperature [7], pH [8,9], ionic strength [10], or light [11] makes those colloids interesting candidates for application as container systems for catalysts [12], payload, or drugs [13]. The most widely studied microgel system is based on the functional polymer poly(*N*-isopropylacrylamide) (PNIPAM) cross-linked with the covalent cross-linker *N,N′*-methylenbis-(acrylamide) (BIS). The chemical cross-linker is added during precipitation polymerization to generate permanent cross-links [7,14]. The thermoresponsive polymer exhibits a lower critical solution temperature (LCST) of approximately 32 °C [15]. Poly(*N*-Vinylcaprolactam) (PVCL) is another thermoresponsive polymer with a similar LCST. It has the advantage of showing high resistance against hydrolysis and low toxicity, making it more biocompatible, which makes it interesting to utilize as a building block in biomaterials [15,16].

However, besides chemical cross-linking, cross-linking can also be of physical origin. Non-covalent cross-linking is more commonly found in the preparation of hydrogels, but there are also examples of the use of non-covalent interactions for the cross-linking of microgels [17]. Physical cross-linking often provides a more dynamic network offering new properties in microgels, such as stimuli-responsive degradation, enhanced drug release control, enhanced catalytic activity, or the formation of supracolloidal assemblies [18–20]. Cross-linking through supramolecular interactions in microgels is often realized by a combination of non-covalent interactions such as hydrogen bonding, π-π stacking, electrostatic interactions, coordination, and hydrophobic effects. In the past, our group exploited physical cross-linking to fabricate PVCL-based microgels via hydrogen bonding using tannic acid, and via host-guest interactions using methacrylate-modified β-cyclodextrin and vinyl ferrocene. Most recently, we demonstrated that the transformation of random coils into ordered β-sheets can drive the formation of sugar beet pectin and silk fibroin-based microgels [18,19,21]. Furthermore, there are other examples of non-covalently-cross-linked microgels involving host-guest interactions [20,22] or multiple hydrogen bonds [23]. For example, Wöll et al. reported the synthesis of PNIPAM microgels with supramolecular crosslinks achieved by host-guest interactions between trans azobenzene and β-cyclodextrin, allowing the volume phase transition temperature (VPTT) to change upon irradiation [22]. Supramolecular crosslinking is also applied for the interlinking of several microgels, for example, leading to reversible assemblies of PNIPAM-based microgels through host-guest interactions or metal complexation [24,25].

Peptides can self-assemble, and they are, due to their simple structure, ideal candidates for the bottom-up fabrication of complex nanostructures. They occur abundantly in nature, where they are found to be involved in many physiological processes. Due to their diverse array of unique properties and straightforward structure and synthesis, peptides are highly promising candidates for the development of functional materials. Another advantage is their biocompatibility and ability to be biodegradable [26,27]. The self-assembly of short peptides has been extensively researched, as they can form complex, functional nanostructures. *L*-phenylalanyl-*L*-phenylalanine (Phe-Phe) is a widely explored aromatic dipeptide building block [28–30]. Based on the Phe-Phe building block diphenylalanine, the smallest self-assembling peptide sequence derived from the Alzheimer's β-amyloid core recognition motif has emerged as a keystone in the study of peptide-based nanostructures. Its ability to self-assemble into diverse morphologies, such as nanotubes, spheres, plates, and hydrogels, results from non-covalent interactions [29–33]. The assembly of the Phe-Phe motif is primarily driven by hydrogen bonding and π-π stacking interactions between its aromatic residues, with additional contributions from hydrophobic interactions and van der Waals forces [34]. The self-assembly process of the dipeptides is influenced by factors such as hydrophobicity, temperature, pH, or peptide concentration [35]. Phe-Phe-based nanostructures have been utilized, among other fields, in energy storage [36,37], as biosensors [38,39], in wound healing and tissue engineering [40,41], and as drug delivery systems [42–44].

Most studies focus on the development of bio-inspired nanomaterials by using supramolecular interactions between elementary building blocks, but only a few have explored using the Phe-Phe motif in a monomer for synthesizing polymers and nanoparticles via (controlled) radical polymerization with Phe-Phe moieties in the side chain [45–49]. Skaat et al. reported the synthesis of polymeric nanoparticles from an *N*-acryloyl amino acid monomer possessing the Phe-Phe motif via dispersion polymerization [45]. Warren et al. synthesized Phe-Phe-based random amphiphilic copolymers via controlled radical polymerization, demonstrating how hydrophobic forces drive global collapse and β-sheet-like structures [49]. A similar monomer has been utilized by Yonenuma et al. in combination with NIPAM to synthesize random and block copolymers using controlled radical polymerization [47]. However, the fabrication of microgels using the self-assembling Phe-Phe dipeptide motif has, until now, remained unexplored.

In this work, we exploit the Phe-Phe dipeptide motif, particularly the π-π stacking of its aromatic rings, as a physical cross-linker to fabricate thermoresponsive microgels. A variety of PVCL-based microgels with different chemical compositions, sizes, and morphologies were synthesized via precipitation polymerization using a Phe-Phe-based comonomer as the physical cross-linker. These physically cross-linked microgels were compared to their chemically (BIS) cross-linked counterparts and hybrid microgels containing both physical and chemical cross-links. The monomer *N*-acryloyl-*L*-phenylalanyl-*L*-phenylalanine methyl ester (A-Phe-Phe-Me) and the amount incorporated into the microgel structures during synthesis were analyzed using nuclear magnetic resonance (^{1}H NMR). Fourier-transform infrared (FTIR) and Raman spectroscopy were used to further study the chemical composition of the monomers and microgels. The temperature-responsiveness of the microgels was assessed using dynamic light scattering (DLS), while circular dichroism (CD) spectroscopy was used to investigate aromatic π-π stacking. Furthermore, organic solvent (tetrahydrofuran (THF))-induced degradation, resulting from the disruption of physical cross-linking, was examined via scanning electron microscopy (SEM) and DLS. Finally, the effect of dipeptide concentration on morphological changes was established.

2. Results and discussion

2.1. Synthesis and chemical composition

The objective of this work was to synthesize supramolecularly cross-linked microgels by self-assembly of peptide motifs using precipitation polymerization. Therefore, a Phe-Phe derivative comonomer, *N*-acryloyl-*L*-phenylalanyl-*L*-phenylalanine methyl ester (A-Phe-Phe-Me), was synthesized according to the literature to introduce a double bond for radical polymerization via esterification and acryloyl substitution

starting from Phe-Phe (Fig. 1a) [48,50]. It is important to note that *N*-vinylcaprolactam (VCL), unlike *N*-isopropylacrylamide (NIPAM), cannot self-crosslink during the free radical polymerization process, making the use of additional cross-linkers essential for forming stable microgels [51,52]. In total, three different PVCL-based microgel systems were evaluated: one utilizing the covalent cross-linker *N,N′*-methylenebis(acrylamide) (BIS), another employing A-Phe-Phe-Me as a physical cross-linker, and a third incorporating a combination of both cross-linkers. (Fig. 1b). A total of 5 mol% cross-linker with 95 mol% VCL was utilized for all three systems, yielding a total concentration of 0.16 mmol mL^{-1}. In cases where both chemical and physical cross-linkers were combined, each was employed at a ratio of 2.5 mol%. Due to the low water solubility of A-Phe-Phe-Me, it was pre-dissolved in dimethyl sulfoxide (DMSO), resulting in a final DMSO concentration of 10 v%. Our previous studies showed that solvent concentration is a crucial parameter influencing the incorporation efficiency of hydrophobic co-monomers. Although higher amounts of organic solvents facilitate the polymerization of hydrophobic comonomers, they can also promote the formation of secondary particles and decrease the formation of VCL microgels [53]. The reaction is initiated by adding 0.2 mol% of a water-soluble initiator at 70 °C. Herby, PVCL-*co*-A-Phe-Phe-Me chains are formed in a precipitated state, creating microgel nuclei due to the temperature-responsiveness of PVCL. The π-π interactions between the phenylalanine rings of the Phe-Phe motif, along with hydrogen bonding across polymer chains, lead to the formation of colloidally stable microgels with physical cross-links, which will be further discussed throughout this paper. Dialysis was employed to remove low-molecular-weight oligomers and residual reactants from the microgel dispersions (12–14 kDa molecular weight cut-off). To quantitatively investigate the presence of higher-molecular-weight water-soluble species, centrifugation and collection of the supernatant can be used for microgels. Therefore, a systematic fractionation study was conducted via high-speed centrifugation on representative microgel dispersions (5 and 20 mol% A-Phe-Phe-Me). Centrifugation at a relative centrifugal force (RCF) of 16.800 x g resulted in a significant mass fraction remaining in the supernatant (49 and 24%, respectively), determined gravimetrically after lyophilization. However, analysis revealed that this fraction does not consist of dissolved linear polymer chains. Specifically, dynamic light scattering (DLS) and atomic force microscopy (AFM) of the supernatant confirmed the presence of discrete, spherical colloidal particles (Fig. S1a-d, supporting information (SI)). Ultracentrifugation at 80.000 x*g* was performed, leading to recovered mass fractions of 48 and 70%. However, this fraction also does not consist solely of dissolved, water-soluble polymeric species, but rather represents a bimodal distribution of small microgel precursors and fragments. The significant increase in the supernatant mass fraction, combined with the loss of defined spherical morphology and thermoresponsiveness, suggests that the supramolecular network may undergo mechanical fragmentation under extreme centrifugal fields. DLS measurements at 20 and 50 °C revealed a bimodal population of particles with hydrodynamic diameters between 40 and 220 nm (Fig. S2a-b, SI). Furthermore, AFM images reveal the presence of microgel fragments (Fig. S2c-d, SI). Therefore, this method is not adequate to quantitatively determine the exact amount of water-soluble polymer for this microgel system. All subsequent studies were performed using the dialyzed microgel dispersions.

The objective of this work was to synthesize supramolecularly cross-linked microgels by self-assembly of peptide motifs using precipitation polymerization. Therefore, a Phe-Phe derivative comonomer, *N*-acryloyl-*L*-phenylalanyl-*L*-phenylalanine methyl ester (A-Phe-Phe-Me), was synthesized according to the literature to introduce a double bond for radical polymerization via esterification and acryloyl substitution starting from Phe-Phe (Fig. 1a) [48,50]. It is important to note that *N*-vinylcaprolactam (VCL), unlike *N*-isopropylacrylamide (NIPAM), cannot self-crosslink during the free radical polymerization process, making the use of additional cross-linkers essential for forming stable microgels [51,52]. In total, three different PVCL-based microgel systems were evaluated: one utilizing the covalent cross-linker *N,N′*-methylenebis(acrylamide) (BIS), another employing A-Phe-Phe-Me as a physical cross-linker, and a third incorporating a combination of both cross-linkers. (Fig. 1b). A total of 5 mol% cross-linker with 95 mol% VCL was utilized for all three systems, yielding a total concentration of 0.16 mmol mL^{-1}. In cases where both chemical and physical cross-linkers were combined, each was employed at a ratio of 2.5 mol%. Due to the low water solubility of A-Phe-Phe-Me, it was pre-dissolved in dimethyl sulfoxide (DMSO), resulting in a final DMSO concentration of 10 v%. Our previous studies showed that solvent concentration is a crucial parameter influencing the incorporation efficiency of hydrophobic co-monomers. Although higher amounts of organic solvents facilitate the polymerization of hydrophobic comonomers, they can also promote the formation of secondary particles and decrease the formation of VCL microgels [53]. The reaction is initiated by adding 0.2 mol% of a water-soluble initiator at 70 °C. Herby, PVCL-*co*-A-Phe-Phe-Me chains are formed in a precipitated state, creating microgel nuclei due to the temperature-responsiveness of PVCL. The π-π interactions between the phenylalanine rings of the Phe-Phe motif, along with hydrogen bonding across polymer chains, lead to the formation of colloidally stable microgels with physical cross-links, which will be further discussed throughout this paper. Dialysis was employed to remove low-molecular-weight oligomers and residual reactants from the microgel dispersions (12–14 kDa molecular weight cut-off). To quantitatively investigate the presence of higher-molecular-weight water-soluble species, centrifugation and collection of the supernatant can be used for microgels. Therefore, a systematic fractionation study was conducted via high-speed centrifugation on representative microgel dispersions (5 and 20 mol% A-Phe-Phe-Me). Centrifugation at a relative centrifugal force (RCF) of 16.800 x g resulted in a significant mass fraction remaining in the supernatant (49 and 24%, respectively), determined gravimetrically after lyophilization. However, analysis revealed that this fraction does not consist of dissolved linear polymer chains. Specifically, dynamic light scattering (DLS) and atomic force microscopy (AFM) of the supernatant confirmed the presence of discrete, spherical colloidal particles (Fig. S1a-d, supporting information (SI)). Ultracentrifugation at 80.000 x*g* was performed, leading to recovered mass fractions of 48 and 70%. However, this fraction also does not consist solely of dissolved, water-soluble polymeric species, but rather represents a bimodal distribution of small microgel precursors and fragments. The significant increase in the supernatant mass fraction, combined with the loss of defined spherical morphology and thermoresponsiveness, suggests that the supramolecular network may undergo mechanical fragmentation under extreme centrifugal fields. DLS measurements at 20 and 50 °C revealed a bimodal population of particles with hydrodynamic diameters between 40 and 220 nm (Fig. S2a-b, SI). Furthermore, AFM images reveal the presence of microgel fragments (Fig. S2c-d, SI). Therefore, this method is not adequate to quantitatively determine the exact amount of water-soluble polymer for this microgel system. All subsequent studies were performed using the dialyzed microgel dispersions.

The chemical composition of the microgels was characterized by Fourier-transform infrared (FTIR), Raman, and nuclear magnetic resonance (^{1}H NMR) spectroscopy. The FTIR spectra of the PVCL-*co*-BIS microgel only show the lactam carbonyl stretching vibration from VCL at 1620 cm^{-1}, whereas the PVCL-*co*-A-Phe-Phe-Me microgel shows additionally the ester carbonyl stretching vibration band of A-Phe-Phe-Me at 1744 cm^{-1}, while the amide carbonyl stretching vibration band overlaps with the one from VCL (Fig. S5, SI). Additionally, a red shift in the ester carbonyl stretching vibration band from 1756 cm^{-1} (associated with the A-Phe-Phe-Me monomer) toward a lower wavenumber of 1744 cm^{-1} shows a weakening of the bond, indicating increased hydrogen bonding involving the carbonyl group [54]. This indicates that the Phe-Phe moieties within the polymer chain could interact, facilitating self-assembly. Furthermore, the Raman spectra of the PVCL-*co*-A-Phe-Phe-

Me microgel show, aside from the VCL signals, additional peaks at 3059 cm^{-1} corresponding to the N—H stretching of A-Phe-Phe-Me and signals at around 1600 cm^{-1} associated with the aromatic C═C bonds of the phenyl groups (Fig. S6, SI). The carbonyl stretching vibration bands from both monomers are similar to the FTIR spectra, with lower intensity. The NMR spectra of the PVCL-*co*-A-Phe-Phe-Me microgel exhibit a broadening of the aromatic signals at 7.2 ppm and the disappearance of the acrylic double bond signals between 5.5 and 6.5 ppm, attributed to the A-Phe-Phe-Me monomer in the monomer spectra. Together with the presence of all characteristic PVCL signals, it qualitatively proves the successful incorporation of A-Phe-Phe-Me (Fig. S3, SI). In conclusion, all three methods show qualitatively the successful incorporation of A-Phe-Phe-Me.

The chemical composition of the microgels was characterized by Fourier-transform infrared (FTIR), Raman, and nuclear magnetic resonance (^{1}H NMR) spectroscopy. The FTIR spectrum of the PVCL-*co*-BIS microgel only shows the lactam carbonyl stretching vibration from VCL at 1620 cm^{-1}, whereas the PVCL-*co*-A-Phe-Phe-Me microgel spectrum shows additionally the ester carbonyl stretching vibration band of A-Phe-Phe-Me at 1744 cm^{-1}, while the amide carbonyl stretching vibration band overlaps with the one from VCL (Fig. S5, SI). Additionally, a red shift in the ester carbonyl stretching vibration band from 1756 cm^{-1} (associated with the A-Phe-Phe-Me monomer) toward a lower wavenumber of 1744 cm^{-1} shows a weakening of the bond, indicating increased hydrogen bonding involving the carbonyl group [54]. This indicates that the Phe-Phe moieties within the polymer chain could interact, facilitating self-assembly. Furthermore, the Raman spectrum of the PVCL-*co*-A-Phe-Phe-Me microgel shows, aside from the VCL signals, additional peaks at 3059 cm^{-1} corresponding to the N—H stretching of A-Phe-Phe-Me and signals at around 1600 cm^{-1} associated with the aromatic C═C bonds of the phenyl groups (Fig. S6, SI). The carbonyl stretching vibration bands from both monomers are similar to the FTIR spectra, with lower intensity. The NMR spectrum of the PVCL-*co*-A-Phe-Phe-Me microgel exhibits a broadening of the aromatic signals at 7.2 ppm and the disappearance of the acrylic double bond signals between 5.5 and 6.5 ppm, attributed to the A-Phe-Phe-Me monomer in the monomer spectrum. Together with the presence of all characteristic PVCL signals, it qualitatively proves the successful incorporation of A-Phe-Phe-Me (Fig. S3, SI). In conclusion, all three methods show qualitatively the successful incorporation of A-Phe-Phe-Me.

In order to assess the amount of A-Phe-Phe-Me incorporated during the synthesis, quantitative ^{1}H NMR studies were performed by using the internal standard dimethyl terephthalate (DMT) in deuterated DMSO to prevent overlapping of the chloroform peak with the aromatic signals (Fig. S4, SI). For microgels targeting 5 mol% A-Phe-Phe-Me, the experimentally determined incorporation of 4.2 mol% aligns well with the targeted value. However, utilizing only 5 v% DMSO instead of 10% during synthesis significantly decreased the incorporation of A-Phe-Phe-Me, reducing it from 4.2 to 2.6 mol% (Table S1, SI). Furthermore, when incorporating both cross-linking types, the experimental amount of A-Phe-Phe-Me was only 0.6 mol% compared to the target of 2.5 mol% (Table S1, SI). The low reactivity of A-Phe-Phe-Me could result from its bulky structure and greater hydrophobicity compared to BIS, causing steric hindrance.

In order to assess the amount of A-Phe-Phe-Me incorporated during the synthesis, quantitative ^{1}H NMR studies were performed by using the internal standard dimethyl terephthalate (DMT) in deuterated DMSO to prevent overlapping of the chloroform peak with the aromatic signals (Fig. S4, SI). For microgels targeting 5 mol% A-Phe-Phe-Me, the experimentally determined incorporation of 4.2 mol% aligns well with the targeted value. However, utilizing only 5 v% DMSO instead of 10% during synthesis significantly decreased the incorporation of A-Phe-Phe-Me, reducing it from 4.2 to 2.6 mol% (Table S1, SI). Furthermore, when incorporating both cross-linking types, the experimental amount of A-Phe-Phe-Me was only 0.6 mol% compared to the target of 2.5 mol% (Table S1, SI). The low reactivity of A-Phe-Phe-Me could result from its bulky structure and greater hydrophobicity compared to BIS, causing steric hindrance.

2.2. Size and morphology study

To investigate the influence of the physical cross-linking on the colloidal stability, size, and temperature sensitivity of the microgels, DLS and scanning transmission electron microscopy (SEM) were performed (Fig. 2). Therefore, the hydrodynamic diameter (D_h) was measured in the swollen and collapsed states at 20 °C ($D_{h,20\ °C}$) and 50 °C ($D_{h,50\ °C}$), respectively. Comparing the three microgel systems reveals that all are in a similar size range of 600 to 700 nm in $D_{h,20\ °C}$ and between 300 and 400 nm in $D_{h,50\ °C}$ (Fig. 2a). A summary of size and polydispersity index (PDI) can be found in the SI (Table S2). With PDI values consistently below 0.01, all three microgel systems prepared are demonstrably highly monodisperse. This suggests that the overall microgel size is only minimally influenced by the type of cross-linking. Additionally, physical cross-linking results in colloidally stable microgels comparable to those formed through chemical cross-linking with narrow size distributions. The swelling ratios (SR) were determined for all systems (Eq. (S1)) from the hydrodynamic diameters below and above the VPTT. The SR (11) was observed for microgels containing only physical crosslinks. In comparison, microgels featuring both crosslinks and those with only covalent crosslinks display reduced ratios of 4.5 and 5.8, respectively. This result suggests slightly higher network flexibility for the physically cross-linked microgels.

To investigate the influence of the physical cross-linking on the colloidal stability, size, and temperature sensitivity of the microgels, DLS and scanning transmission electron microscopy (SEM) were performed (Fig. 2). Therefore, the hydrodynamic diameter (D_h) was measured in the swollen and collapsed states at 20 °C ($D_{h,20\ °C}$) and 50 °C ($D_{h,50\ °C}$), respectively. Comparing the three microgel systems reveals that all are in a similar size range of 600 to 700 nm in $D_{h,20\ °C}$ and between 300 and 400 nm in $D_{h,50\ °C}$ (Fig. 2a). A summary of size and polydispersity index (PDI) can be found in the SI (Table S2). With PDI values consistently below 0.01, all three microgel systems prepared are demonstrably highly monodisperse. This suggests that the overall microgel size is only minimally influenced by the type of cross-linking. Additionally, physical cross-linking results in colloidally stable microgels comparable to those formed through chemical cross-linking with narrow size distributions. The swelling ratios (SR) were determined for all systems (Eq. (S1)) from the hydrodynamic diameters below and above the VPTT. The SR (11.0) was observed for microgels containing only physical crosslinks. In comparison, microgels featuring both crosslinks and those with only covalent crosslinks display reduced ratios of 4.5 and 5.9, respectively. This result suggests slightly higher network flexibility for the physically cross-linked microgels.

To gain deeper insights into the effects of A-Phe-Phe-Me on the size and swelling behavior, the microgel system with solely physical cross-linking was further investigated with a focus on the monomer composition. Microgels with tunable comonomer ratios were synthesized, targeting 0.5 to 50 mol% A-Phe-Phe-Me. Quantitative ^{1}H NMR measurements revealed that the experimental A-Phe-Phe-Me amounts are in good agreement with the targeted ones (Fig. 2c). However, the sample with a target of 50 mol% A-Phe-Phe-Me shows a significantly lower amount of 37.7 mol% incorporated comonomer. The $D_{h,20\ °C}$ increases for the microgels targeting 0.5 to 5.0 mol% A-Phe-Phe-Me from 446 to 649 nm. The microgels targeting 20 and 50 mol% A-Phe-Phe-Me are significantly smaller, with 314 nm and 296 nm, respectively (Table 1, Fig. 2b). In the collapsed state, the $D_{h,50\ °C}$ ranges from 250 to 300 nm for the microgels targeting 0.5 to 5.0 mol% A-Phe-Phe-Me, which is significantly smaller and comparable to the chemically cross-linked microgels. Interestingly, microgels targeting 20 and 50 mol% A-Phe-Phe-Me do not show a size decrease at 50 °C, indicating that higher A-Phe-Phe-Me incorporation increases polymer network stiffness. However, later temperature-dependent heating and cooling cycles (Fig. 3)

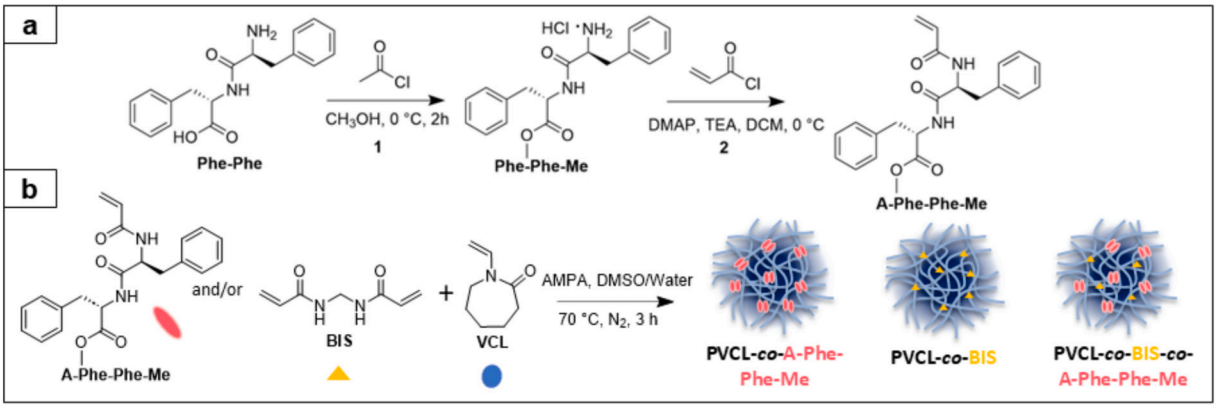

Fig. 1. Synthesis of A-Phe-Phe-Me monomer and microgels. (a) Synthesis scheme of the Phe-Phe-based monomer starting from Phe-Phe: 1. Esterification to form Phe-Phe-Me, and 2. Acryloyl substitution to yield A-Phe-Phe-Me. (b) Microgel synthesis of three distinct PVCL-based microgel structures through chemical and/or physical cross-linking using A-Phe-Phe-Me and BIS.

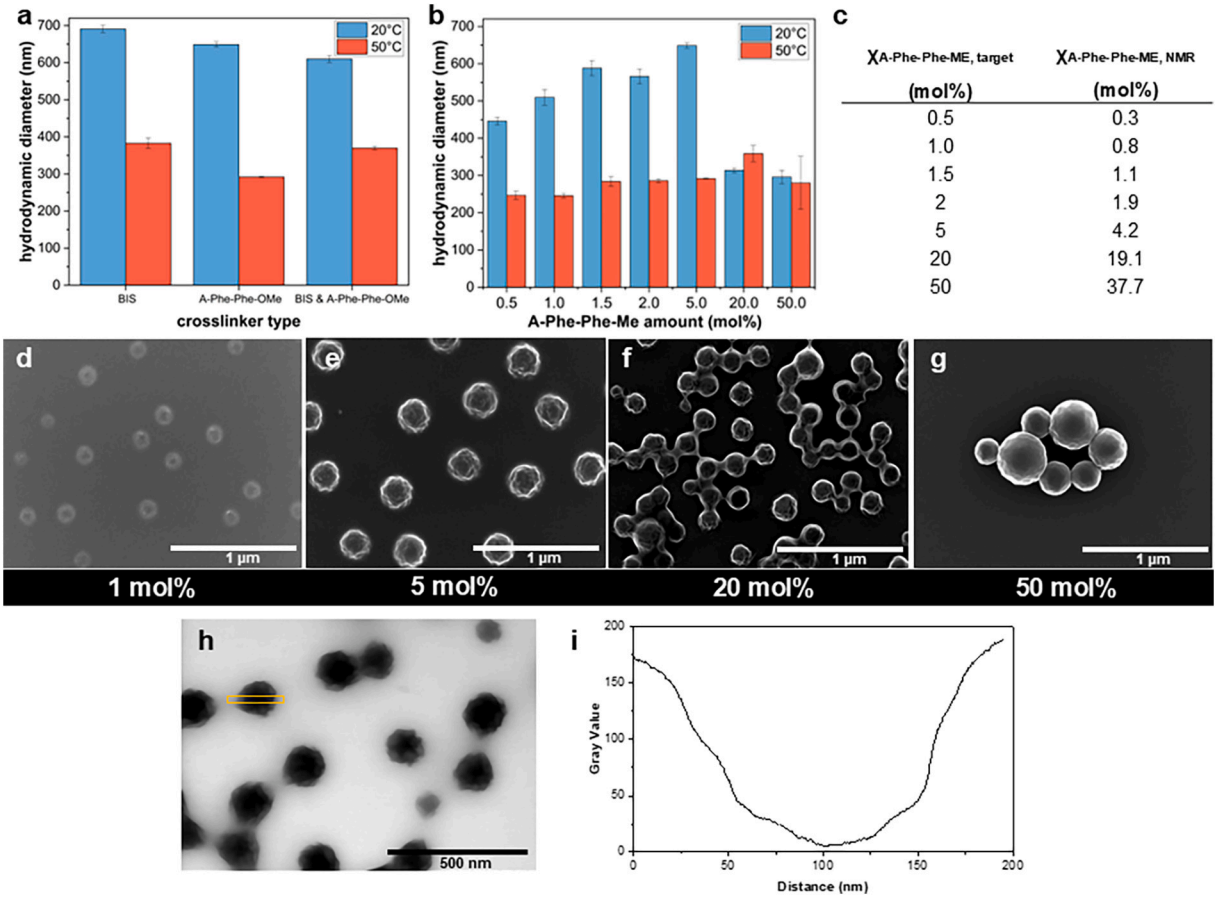

Fig. 2. Size, composition, and morphology analysis of physically and chemically cross-linked microgels. (a) Hydrodynamic diameter of microgels with different cross-linker types at 20 and 50 °C. (b) Hydrodynamic diameter of microgels with A-Phe-Phe-Me amounts between 0.5 and 50 mol% at 20 and 50 °C. Each value represents the average of four replicate measurements. (c) Table of targeted and experimental A-Phe-Phe-Me ratios determined from NMR. (d-g) SEM images of PVCL-*co*-A-Phe-Phe-Me microgels with increasing monomer ratio from left to right. (h) SEM image of 20 mol% PVCL-*co*-A-Phe-Phe-Me microgels. (i) Corresponding grey value profile of a single microgel. The yellow square indicates the region used for applying the grey value profile analysis. (For interpretation of the references to colour in this figure legend, the reader is referred to the web version of this article.)

reveal that this could be due to a kinetic effect, which is discussed later. Furthermore, the increased hydrophobicity can reduce hydration, thereby diminishing the extent of size change in response to temperature variations. However, the substantial increase of the arrow bars, especially for the microgels targeting 50 mol% A-Phe-Phe-Me, also indicates particle agglomeration. Furthermore, the PDI is significantly larger for those microgels (Table 1).

The yield of the synthesized microgels was determined gravimetrically after lyophilizing the purified microgels, which had been filtered to remove larger aggregates and dialyzed to remove low molecular weight

Table 1
Hydrodynamic diameters D_h and PDIs obtained by DLS at 20 and 50 °C of the PVCL-*co*-A-Phe-Phe-Me microgels with increasing A-Phe-Phe-Me ratios. The SR were calculated from the $D_{h,20\ °C}$ and $D_{h,50\ °C}$ using Eq. (S1) (SI).
Hydrodynamic diameters D_h and PDIs obtained by DLS at 20 and 50 °C of the PVCL-*co*-A-Phe-Phe-Me microgels with increasing A-Phe-Phe-Me ratios. The SR were calculated from the $D_{h,20\ °C}$ and $D_{h,50\ °C}$ using Eq. (S1) (SI).

$\chi_{A\text{-}Phe\text{-}Phe\text{-}Me,target}$	$D_{h,20\ °C}$	$D_{h,50\ °C}$	PDI $_{20°C}$	PDI $_{50°C}$	SR
Mol%	(nm)	(nm)	(−)	(−)	(−)
0.5	446 ± 11	247 ± 11	0.29 ± 0.01	0.03 ± 0.02	5.9
1	510 ± 21	246 ± 6	0.13 ± 0.02	0.07 ± 0.02	8.9
1.5	588 ± 20	284 ± 13	0.10 ± 0.04	0.07 ± 0.02	8.9
2	566 ± 20	286 ± 6	0.04 ± 0.04	0.07 ± 0.03	7.8
5	649 ± 7	292 ± 1	0.02 ± 0.02	0.01 ± 0.01	11.0
20	314 ± 7	359 ± 22	0.04 ± 0.02	0.07 ± 0.06	0.7
50	296 ± 18	280 ± 71	0.21 ± 0.03	0.38 ± 0.28	1.1

oligomers and monomer residues. The yield of the microgels targeting between 0.5 and 5 mol% lies between 96 and 82%. However, a significant decrease is noticeable with increasing A-Phe-Phe-Me target amounts of 20 and 50 mol% (Table S1, SI). This is in accordance with the reduced A-Phe-Phe-Me content at higher ratios and can be explained by the hydrophobic character of the comonomer and resulting precipitation from the solution with an increased ratio. Furthermore, as mentioned in Section 2.1, the bulky structure of A-Phe-Phe-Me could hinder the reaction and, therefore, decrease the overall yield. Additionally, the higher A-Phe-Phe-Me amounts can lead to agglomeration of the microgels due to the hydrophobicity of the comonomer. On the other side, aggregation could arise from π-π interactions of the Phe-Phe-moieties across several microgels. The morphology of those microgels with compositions of 1, 5, 20, and 50 mol% is visualized in Fig. 2d-g using SEM. The SEM images underline the previous statement since separate microgels are visible for the microgels with 1 and 5 mol%, while for the ones with 20 and 50 mol%, the microgels show aggregation. However, it is important to note that SEM images only represent the microgels in the dry state.

The yield of the synthesized microgels was determined gravimetrically after lyophilizing the purified microgels, which had been filtered to remove larger aggregates and dialyzed to remove low molecular weight oligomers and monomer residues. The yield of the microgels targeting between 0.5 and 5 mol% lies between 96 and 82%. However, a significant decrease is noticeable with increasing A-Phe-Phe-Me target amounts of 20 and 50 mol% (Table S1, SI). This is in accordance with the reduced A-Phe-Phe-Me content at higher ratios and can be explained by the hydrophobic character of the comonomer and resulting precipitation from the solution with an increased ratio. Furthermore, as mentioned in Section 2.1, the bulky structure of A-Phe-Phe-Me could hinder the reaction and, therefore, decrease the overall yield. Additionally, the higher A-Phe-Phe-Me amounts can lead to agglomeration of the microgels due to the hydrophobicity of the comonomer. On the other side, aggregation could arise from π-π interactions of the Phe-Phe-moieties across several microgels. The morphology of those microgels with compositions of 1, 5, 20, and 50 mol% is visualized in Fig. 2d-g using SEM. The SEM images underline the previous statement since separate microgels are visible for the microgels with 1 and 5 mol%, while for the ones with 20 and 50 mol%, the microgels show aggregation. However, it is important to note that SEM images only represent the microgels in the dry state.

The cross-linker distribution within the microgels strongly determines their network microstructure and thus influences their properties. The observed microgel sizes and swelling ratios between 0.5 and 5.0 mol% A-Phe-Phe-Me ratios deviate from the expected monotonic

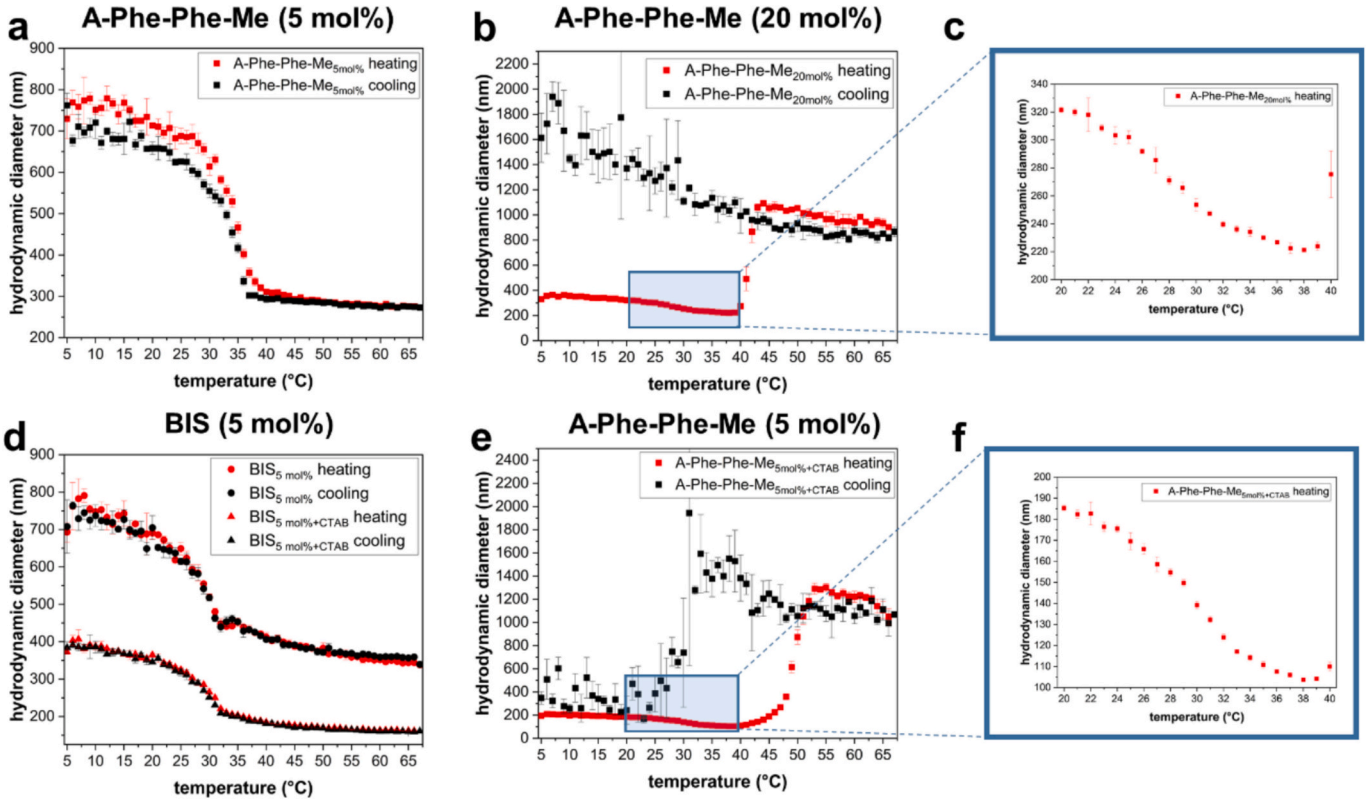

Fig. 3. Hydrodynamic diameters of microgels measured by DLS during temperature-dependent heating and cooling cycles from 5 to 67 °C. (a, b) Microgels cross-linked by A-Phe-Phe-Me using 5 and 20 mol%, respectively. (c) Enlarged view of the heating cycle between 20 and 40 °C of the 20 mol% microgels. (d) Comparison of small and large microgels cross-linked with 5 mol% BIS and addition of CTAB. (e) Small microgels prepared with 5 mol% A-Phe-Phe-Me and CTAB. (f) Enlarged view of the heating cycle between 20 and 40 °C of the 5 mol% + CTAB microgels. Each value represents the average of three replicate measurements.

decrease despite the increase in crosslinker content. This non-monotonicity is likely attributed to the structural impact of low cross-linker concentrations (0.5 to 5.0 mol%). Specifically, the crosslinker distributes differently within the microgel at these small ratios, which, in turn, influences the hydrodynamic radius. In the case of PVCL microgels cross-linked by BIS it has been observed in the past, that the absolute size of the microgel particles, measured by DLS, increases with the increase of cross-linker amount, which is not observed for PNIPAM microgels [55]. The examined regime was between 1.6 and 6.1 mol% (related to the total monomer amount) and is therefore comparable to the regime in this study. Thus, the standard theory correlating increased crosslinker ratio with reduced swelling, determined by DLS, is only applicable beyond a threshold crosslinker concentration and might also apply to this system [56]. For the high crosslinker amounts a significant decrease in size and swelling degree is noticeable.

The cross-linker distribution within the microgel is also dependent on the differences in hydrophobicity between the components. While VCL is water-soluble at the reaction temperature, the A-Phe-Phe-Me cross-linker is significantly more hydrophobic. This high hydrophobicity is expected to cause the cross-linker to preferentially partition into the growing polymer particle after nucleation step during precipitation polymerization. This partitioning effect dictates that the concentration of the cross-linker is highest in the core of the newly formed particle and decreases radially outward. Therefore, a non-homogeneous structure characterized by a highly cross-linked, dense core and a less cross-linked, more diffuse shell is hypothesized. To support this hypothesis, bright-field scanning transmission electron microscopy (BF-STEM) images were recorded to give qualitative insights into the microgels microstructure. In Fig. 2h, a corresponding STEM image of the microgel with 20 mol% A-Phe-Phe-Me is shown. A density gradient within the microgels is clearly visible, indicating a core-shell-like structure. A higher electron density in the central region of the microgels, transitioning to a more diffuse periphery, can be observed. Fig. 2i shows the corresponding grey value profile from the STEM image, obtained from a single microgel, marked by the yellow rectangle. This difference in contrast is indicative of a higher cross-linking density in the particle core. Supplemental STEM images and grey value profiles of the other microgels are included in the SI (Fig. S7). While the microgels containing 1 and 5 mol% A-Phe-Phe-Me show similar density gradients to the ones in Fig. 2h, the microgels with 50 mol% A-Phe-Phe-Me show sharp borders, indicating a more uniform structure and a denser overall particle.

The cross-linker distribution within the microgel is also dependent on the differences in hydrophobicity between the components. While VCL is water-soluble at the reaction temperature, the A-Phe-Phe-Me cross-linker is significantly more hydrophobic. This high hydrophobicity is expected to cause the cross-linker to preferentially partition into the growing polymer particle after nucleation step during precipitation polymerization. This partitioning effect dictates that the concentration of the cross-linker is highest in the core of the newly formed particle and decreases radially outward. Therefore, a non-homogeneous structure characterized by a highly cross-linked, dense core and a less cross-linked, more diffuse shell is hypothesized. To support this hypothesis, bright-field scanning transmission electron microscopy (BF-STEM) images were recorded to give qualitative insights into the microgels microstructure. In Fig. 2h, a corresponding STEM image of the microgel with 20 mol% A-Phe-Phe-Me is shown. A density gradient within the microgels is clearly visible, indicating a core-shell-like structure. A higher electron density in the central region of the microgels, transitioning to a more diffuse periphery, can be observed. Fig. 2i shows the corresponding grey value profile from the STEM image, obtained from a single microgel, marked by the yellow rectangle. This difference in contrast is indicative of a higher cross-linking density in the particle core. Supplemental STEM images and grey value profiles of the other microgels are included in the SI (Fig. S7). While the microgels containing 1 and 5 mol% A-Phe-Phe-Me show similar density gradients to the ones in Fig. 2h, the microgels with 50 mol% A-Phe-Phe-Me show sharp borders, indicating a more uniform structure and a denser overall particle.

To gain a deeper understanding of this behavior, temperature-dependent DLS measurements were performed by heating the samples from 5 to 67 °C and cooling in a reverse manner, which are presented in Fig. 3. The microgels cross-linked with 5 mol% A-Phe-Phe-Me (Fig. 3a) exhibit a similar trend to the ones cross-linked with 5 mol% BIS (Fig. 3d). However, in this case, the physically cross-linked microgels show a sharper transition than the chemically cross-linked ones, suggesting that the physically cross-linked polymer chains have more freedom to undergo cooperative collapse. Furthermore, the physically cross-linked microgels show a small hysteresis and a reduction of the final microgel size in the cooling cycle compared to the heating cycle, indicating that the reswelling process is not fully reversible, which could arise from hydrophobic interactions.

When the amount of A-Phe-Phe-Me is increased to 20 mol%, two effects can be observed from the heating cycle. Firstly, a reduction in size of 100 nm can be observed from 321 nm at 20 °C to 221 nm at 38 °C (Fig. 3c). This reveals that a volume phase transition takes place. This was not apparent in the static size data from the single-point measurements at 20 and 50 °C (Fig. 2b). The size reduction is more gradual compared to the 5 mol% sample. The second effect that can be observed is a sharp increase in D_h at 40 °C (Fig. 3b). However, this apparent size increase is likely due to the aggregation of multiple microgels rather than an actual growth in size. This is further supported by an increase in PDI from around 0.05 to around 0.2 (Fig. S8b, SI). Interestingly, the cooling cycle does not restore the initial microgel size, suggesting that the aggregation is thermally irreversible, possibly due to intermolecular π–π stacking across multiple microgels. Furthermore, the size of the aggregates at 50 °C is significantly larger in the temperature trend measurement compared to the single-point temperature measurement (Fig. 2b). Overall, this can be attributed to a kinetic effect that occurs over the prolonged period during temperature-dependent measurements when the particles are maintained in their collapsed, highly adhesive state (above the VPTT), as one complete heating and cooling cycle takes approximately 14 h. In comparison, the time between the single-point measurements of 20 and 50 °C is only approximately 6 min.

When the amount of A-Phe-Phe-Me is increased to 20 mol%, two effects can be observed from the heating cycle. Firstly, a reduction in size of 100 nm can be observed from 321 nm at 20 °C to 221 nm at 38 °C (Fig. 3c). This reveals that a volume phase transition takes place. This was not apparent in the static size data from the single-point measurements at 20 and 50 °C (Fig. 2b). The size reduction is more gradual compared to the 5 mol% sample. The second effect that can be observed is a sharp increase in D_h at 40 °C (Fig. 3b). However, this apparent size increase is likely due to the aggregation of multiple microgels rather than an actual growth in size. This is further supported by an increase in PDI from around 0.05 to around 0.2 (Fig. S8b, SI). Interestingly, the cooling cycle does not restore the initial microgel size, suggesting that the aggregation is thermally irreversible, possibly due to intermolecular π–π stacking across multiple microgels. Furthermore, the size of the aggregates at 50 °C is significantly larger in the temperature trend measurement compared to the single-point temperature measurement (Fig. 2b). Overall, this can be attributed to a kinetic effect that occurs over the prolonged period during temperature-dependent measurements when the particles are maintained in their collapsed, highly adhesive state (above the VPTT), as one complete heating and cooling cycle takes approximately 14 h. In comparison, the time between the single-point measurements of 20 and 50 °C is only approximately 6 min.

The microgels with 20 mol% A-Phe-Phe-Me are significantly smaller than those with 5 mol%. Therefore, size could also play a crucial role in the formation of aggregates. To investigate this, microgels targeting 5 mol% cross-linker were prepared with the addition of 0.5 mol% of the surfactant cetyltrimethylammonium bromide (CTAB) during the synthesis. Surfactants are, in general, known to decrease the size of

microgels as they act as stabilizers during nuclei formation in precipitation polymerization, depending on the concentration [7]. The surfactant was removed from the dispersion by dialysis after the synthesis. This resulted in A-Phe-Phe-Me cross-linked microgels with a $D_{h,20\ °C}$ of around 200 nm (Fig. 3e). For comparison, BIS cross-linked microgels with a $D_{h,20\ °C}$ of around 400 nm were prepared under the same conditions (Fig. 3d). Interestingly, temperature-dependent DLS measurements reveal that the size of physically cross-linked microgels significantly influences their thermoresponsive behavior. While small BIS cross-linked microgels synthesized with CTAB exhibit similar behavior to their larger counterparts synthesized without CTAB (Fig. 3d), small A-Phe-Phe-Me cross-linked microgels synthesized with CTAB do not mimic their larger counterparts. Instead, their behavior closely resembles that of microgels with a target composition of 20 mol % A-Phe-Phe-Me (Fig. 3e-f). Although the size appears to decrease during the cooling cycle, the persistently high PDI suggests that the aggregates do not disassemble (Fig. S8b, SI). However, unlike the 20 mol % microgels, the smaller 5 mol% microgels exhibit a less pronounced increase in D_h, occurring at higher temperatures (Fig. 3e), as supported by the PDI data (Fig. S8e, SI). This suggests that aggregate formation occurs more gradually at elevated temperatures. To further investigate this behavior, scanning transmission electron microscopy (STEM) images were taken of this sample under different conditions: one was dispersed on the grid at room temperature (RT), while the other was heated to 70 °C and dispersed while hot (Fig. S9a-b, SI). The RT sample exhibits a monodisperse distribution of microgels, whereas the heated sample shows aggregate formation.

The microgels with 20 mol% A-Phe-Phe-Me are significantly smaller than those with 5 mol%. Therefore, size could also play a crucial role in the formation of aggregates. To investigate this, microgels targeting 5 mol% cross-linker were prepared with the addition of 0.5 mol% of the surfactant cetyltrimethylammonium bromide (CTAB) during the synthesis. Surfactants are, in general, known to decrease the size of microgels as they act as stabilizers during nuclei formation in precipitation polymerization, depending on the concentration [7]. The surfactant was removed from the dispersion by dialysis after the synthesis. This resulted in A-Phe-Phe-Me cross-linked microgels with a $D_{h,20\ °C}$ of around 200 nm (Fig. 3e). For comparison, BIS cross-linked microgels with a $D_{h,20\ °C}$ of around 400 nm were prepared under the same conditions (Fig. 3d). Interestingly, temperature-dependent DLS measurements reveal that the size of physically cross-linked microgels significantly influences their thermoresponsive behavior. While small BIS cross-linked microgels synthesized with CTAB exhibit similar behavior to their larger counterparts synthesized without CTAB (Fig. 3d), small A-Phe-Phe-Me cross-linked microgels synthesized with CTAB do not mimic their larger counterparts. Instead, their behavior closely resembles that of microgels with a target composition of 20 mol % A-Phe-Phe-Me (Fig. 3e-f). Although the size appears to decrease during the cooling cycle, the persistently high PDI suggests that the aggregates do not disassemble (Fig. S8b, SI). However, unlike the 20 mol % microgels, the smaller 5 mol% microgels exhibit a less pronounced increase in D_h, occurring at higher temperatures (Fig. 3e), as supported by the PDI data (Fig. S8e, SI). This suggests that aggregate formation occurs more gradually at elevated temperatures. To further investigate this behavior, scanning transmission electron microscopy (STEM) images were taken of this sample under different conditions: one was dispersed on the grid at room temperature (RT), while the other was heated to 70 °C and dispersed while hot (Fig. S9a-b, SI). The RT sample exhibits a monodisperse distribution of microgels, whereas the heated sample shows aggregate formation.

To determine if the observed heat-induced aggregation effects stem from a reduced charge density due to size shrinkage, zeta potential (ζ) measurements above and below the VPTT were performed (Table 2). Contrary to the expected slightly positive ζ (resulting from the positively charged AMPA initiator), the microgels were found to have negative ζ values. This result may be due to the low initiator concentration (0.2 mol % in relation to the monomer content), which is significantly lower than the concentration used in reports showing positive ζ (which, e.g. used 8× higher AMPA amounts) [57]. Therefore, this low charge density may also be subject to shielding effects during the measurement. Upon collapse, the ζ of BIS cross-linked microgels became marginally more negative (from −1 to −6 mV), whereas the A-Phe-Phe-Me cross-linked microgels showed a strong shift to negative values between −23 and − 32 mV. The strong negative ζ suggests that the increased hydrophobicity, resulting from the A-Phe-Phe-Me units and the collapse of the polymer chains, promotes the adsorption of negatively charged ions (such as hydroxide ions) from the surrounding aqueous medium [57]. Therefore, it can be assumed that the aggregation is not due to a reduced charge density. While a highly negative ζ normally indicates strong inter-particle repulsion and ensures colloidal stability, in this specific case, the highly hydrophobic A-Phe-Phe-Me moiety introduces a counteracting hydrophobic attraction between the collapsed polymer chains, which can induce aggregation. The observed heat-induced aggregation may be a consequence of the hydrophobic A-Phe-Phe-Me moiety combined with differences in the SR. Determining the SR from the temperature-dependent heating cycles (at 20 and 38 °C) reveals a significant difference: the large microgels with 5 mol% A-Phe-Phe-Me exhibit an SR of 9.5, which is much larger than their small counterparts with a SR of 5.7. Microgels containing 20 mol% A-Phe-Phe-Me show the lowest SR of 3.1.

Table 2
Zeta potential (ζ) at 20 and 55 °C of different microgels.

Microgel	$\zeta_{20°C}$ (mV)	$\zeta_{55°C}$ (mV)
20 Mol% A-Phe-Phe-me	−2.6 ± 0.7	−29.3 ± 0.7
5 Mol% A-Phe-Phe-me	−7.4 ± 0.7	−32.0 ± 0.8
5 Mol% A-Phe-Phe-me + CTAB	−5.3 ± 1.1	−35.7 ± 0.7
5 Mol% BIS + CTAB	−1.0 ± 0.5	−6.0 ± 1.4

2.3. Time-dependent formation of A-Phe-Phe-me cross-linked microgels

To gain deeper insight into the mechanism of microgel formation, DLS measurements and SEM images were recorded at various time points during the reaction (Fig. 4). Samples were collected during the synthesis of microgels with a monomer ratio of 95 to 5 (VCL to A-Phe-Phe-Me) at times between 1 and 180 min. To stop the polymerization process, the samples were rapidly cooled down and exposed to oxygen. DLS analysis reveals that the microgels grew steadily, reaching a final hydrodynamic diameter of approximately 500 nm after about 30 min (Fig. 4a). This observation aligns well with previous reports made on microgels cross-linked with the covalent cross-linker BIS, which are extensively characterized in the literature [58].

Interestingly, the samples collected at 1- and 3-min display larger hydrodynamic diameters from the DLS measurements compared to those collected at 5 min (Fig. 4a). The PDI of these early-stage samples exceeds 1, which normally indicates heterogeneity. However, these results require caution because PDI measurements under weak scattering conditions, caused by the predominance of small particles after this short time, can be unreliable. In contrast, samples collected at 5 min and later time points are highly monodisperse, with PDIs close to 0 (Fig. 4b). A table of size and PDI value can be found in the SI (Table S4). To complement the DLS data, SEM images were obtained from the samples collected at 3, 5, and 15 min (highlighted in orange in Fig. 4a). The SEM images reveal that, in contrast to the DLS results, the microgels at 3 min are highly monodisperse and significantly smaller than those at 5 and 15 min. The image shows aggregated particles, but this may result from drying artifacts, especially given the presence of unreacted molecules and oligomers in the continuous phase (Fig. 4d-f). The diameters of multiple microgels from SEM images were measured and displayed as a histogram in Fig. 4b. The observed aggregation behavior may indicate a faster reaction of A-Phe-Phe-Me, leading to intramolecular interactions

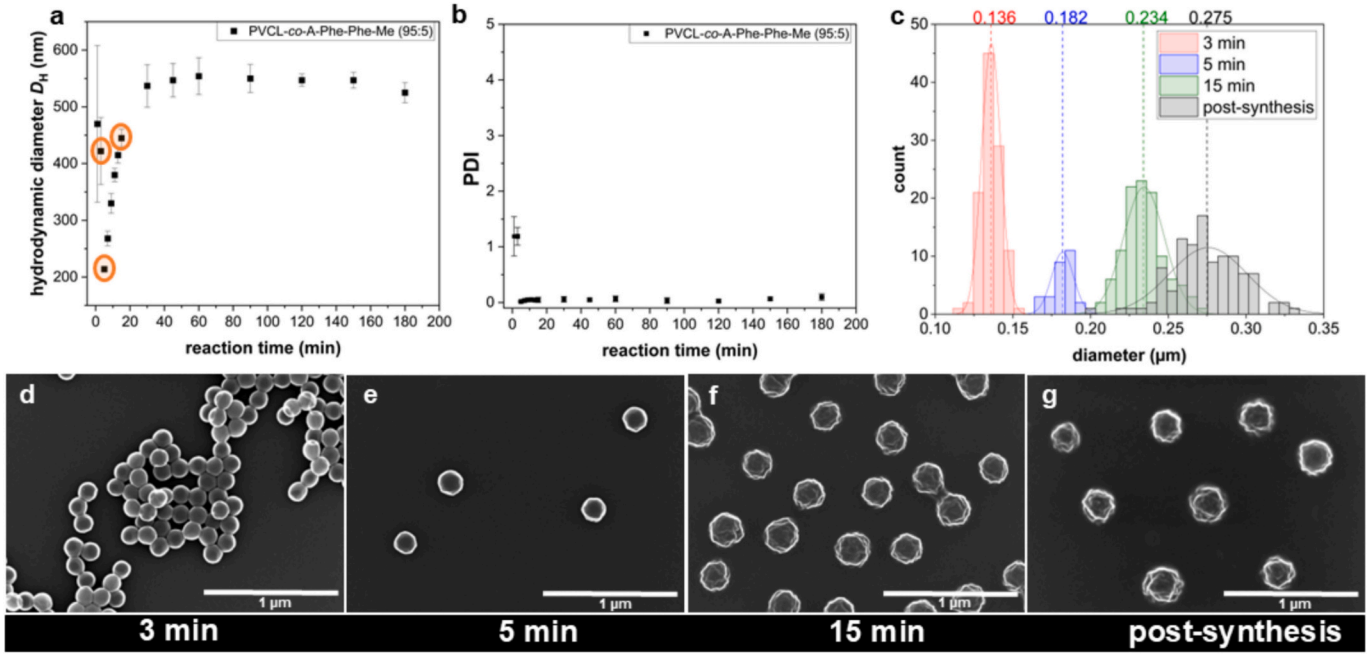

Fig. 4. Time-dependent formation of A-Phe-Phe-Me cross-linked microgels. (a) Hydrodynamic diameter of PVCL-*co*-A-Phe-Phe-Me microgels measured at 20 °C at various time points during the reaction. The orange circles represent the time points at which the SEM analysis was made. (b) Corresponding PDI data to the D_h. Each value represents the average of four replicate measurements. (c) Diameter distribution histogram of microgels measured after 3, 5, and 15 min, as well as post-synthesis, based on multiple SEM images. (d-g) Representative SEM images corresponding to each time point: 3 min (d), 5 min (e), 15 min (f), and post-synthesis (180 min) (g).

between the small precursor microgels as the aromatic groups from A-Phe-Phe-Me are more available on the surface. With increasing reaction time, those agglomerates are broken by the constant stirring of the solution. Additionally, the surface morphology of the particles shows a transition from smooth to increasingly rough surfaces as the reaction progresses. Notably, the post-synthesis microgels display the roughest surface morphology (Fig. 4g).

Interestingly, the samples collected at 1- and 3-min display larger hydrodynamic diameters from the DLS measurements compared to those collected at 5 min (Fig. 4a). The PDI of these early-stage samples exceeds 1, which normally indicates heterogeneity. However, these results require caution because PDI measurements under weak scattering conditions, caused by the predominance of small particles after this short time, can be unreliable. In contrast, samples collected at 5 min and later time points are highly monodisperse, with PDIs close to 0 (Fig. 4b). A table of size and PDI value can be found in the SI (Table S4). To complement the DLS data, SEM images were obtained from the samples collected at 3, 5, and 15 min (highlighted in orange in Fig. 4a). The SEM images reveal that, in contrast to the DLS results, the microgels at 3 min are highly monodisperse and significantly smaller than those at 5 and 15 min. The image shows aggregated particles, but this may result from drying artifacts, especially given the presence of unreacted molecules and oligomers in the continuous phase (Fig. 4d-f). The diameters of multiple microgels from SEM images were measured and displayed as a histogram in Fig. 4b. The observed aggregation behavior may indicate a faster reaction of A-Phe-Phe-Me, leading to intramolecular interactions between the small precursor microgels as the aromatic groups from A-Phe-Phe-Me are more available on the surface. With increasing reaction time, those agglomerates are broken by the constant stirring of the solution. Additionally, the surface morphology of the particles shows a transition from smooth to increasingly rough surfaces as the reaction progresses. Notably, the post-synthesis microgels display the roughest surface morphology (Fig. 4g).

2.4. Investigation of π-π stacking-driven microgel formation

Following the above characterizations, the π-π stacking-driven formation of the microgels was examined using CD spectroscopy. For this, microgels targeting 20 mol% A-Phe-Phe-Me were analyzed at increasing concentrations. A strong positive peak at 226 nm (Fig. 5a) was observed, indicating π-π stacking of the phenylalanine rings within the A-Phe-Phe-Me comonomer. This attribution is supported by previous studies reporting phenylalanine-based aromatic stacking-driven self-assembly, resulting in fibril and hydrogel structures [59–61]. A plot of the circular dichroic signal at 226 nm as a function of microgel concentration exhibits a linear correlation (Fig. 5b), indicating dispersion homogeneity in solution and the absence of aggregation within the examined range of 0.1 to 0.4 mg mL^{-1}. Microgels cross-linked solely by BIS were used as a negative control and exhibited no representative CD signal (Fig. S11f, SI). Subsequently, microgels with a target of 2.5 mol% each of the chemical cross-linker BIS and the physical cross-linker A-Phe-Phe-Me were studied. A strong positive CD signal at 226 nm, which increased linearly with concentration, confirmed the presence of π-π stacking and the homogeneity of the system (Fig. 5c). Lastly, CD spectra of microgels with increasing molar ratios of A-Phe-Phe-Me, measured at a fixed concentration of 0.2 mg mL^{-1}, were recorded. A linear correlation between signal intensity and A-Phe-Phe-Me content was observed (Fig. 5d). Overall, these results demonstrate that microgel formation is driven by π-π stacking.

Following the above characterizations, the π-π stacking-driven formation of the microgels was examined using CD spectroscopy. For this, microgels targeting 20 mol% A-Phe-Phe-Me were analyzed at increasing concentrations. A strong positive peak at 226 nm (Fig. 5a) was observed, indicating π-π stacking of the phenylalanine rings within the A-Phe-Phe-Me comonomer. This attribution is supported by previous studies reporting phenylalanine-based aromatic stacking-driven self-assembly, resulting in fibril and hydrogel structures [59–61]. A plot of the circular dichroic signal at 226 nm as a function of microgel concentration exhibits a linear correlation (Fig. 5b), indicating dispersion homogeneity in solution and the absence of aggregation within the examined range of

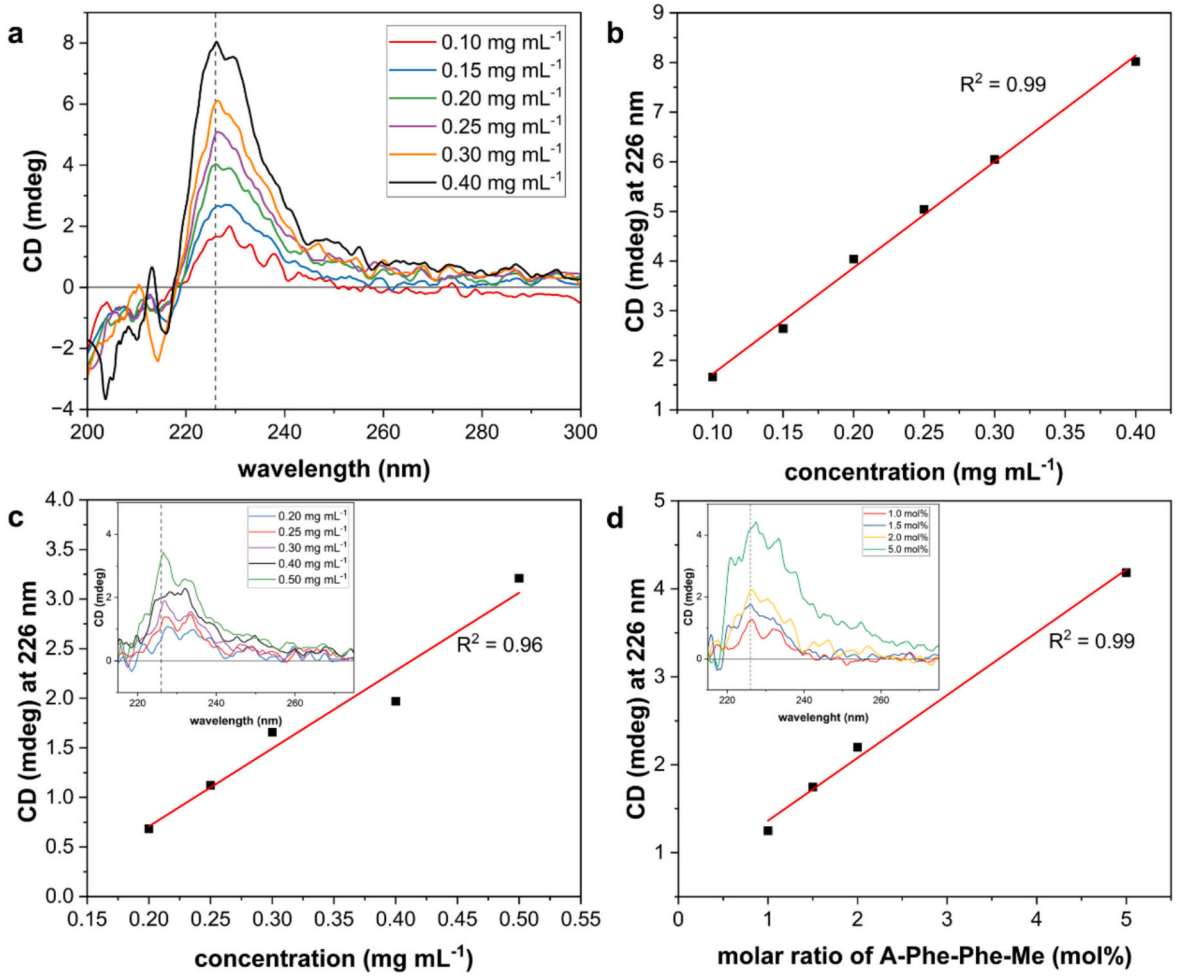

Fig. 5. CD-based analysis of A-Phe-Phe-Me cross-linked microgels. (a) CD spectra of PVCL-*co*-A-Phe-Phe-Me microgel targeting 20 mol% A-Phe-Phe-Me at concentrations ranging from 0.1 to 0.4 mg mL^{-1}. (b) Linear correlation between the circular dichroic signal at 226 nm and microgel concentration. (c) CD spectra and the corresponding linear correlation plot of PVCL-*co*-A-Phe-Phe-Me-*co*-BIS microgels, prepared with 2.5 mol each of BIS and A-Phe-Phe-Me, at concentrations ranging from 0.2 to 0.5 mg mL^{-1}. (d) CD spectra and the corresponding linear correlation plot of PVCL-*co*-A-Phe-Phe-Me microgels with increasing molar ratios of A-Phe-Phe-Me, measured at a fixed microgel concentration. The dotted line in all plots represents the peak at 226 nm. Each spectrum is an average of three accumulations.

0.1 to 0.4 mg mL^{-1}. Microgels cross-linked solely by BIS were used as a negative control and exhibited no representative CD signal (Fig. S11f, SI). Subsequently, microgels with a target of 2.5 mol% each of the chemical cross-linker BIS and the physical cross-linker A-Phe-Phe-Me were studied. A strong positive CD signal at 226 nm, which increased linearly with concentration, confirmed the presence of π-π stacking and the homogeneity of the system (Fig. 5c). Lastly, CD spectra of microgels with increasing molar ratios of A-Phe-Phe-Me, measured at a fixed concentration of 0.2 mg mL^{-1}, were recorded. A linear correlation between signal intensity and A-Phe-Phe-Me content was observed (Fig. 5d). Overall, these results demonstrate that microgel formation is driven by π-π stacking.

Furthermore, the thermal effect on π-π stacking was monitored by recording temperature-dependent CD spectra. A decrease in signal intensity at 226 nm with increasing temperature was observed for microgels (0.2 mg mL^{-1}) targeting 20 mol% A-Phe-Phe-Me (Fig. S11a–b, SI). This is likely a result of microgel aggregation at elevated temperatures, as indicated by a concurrent drop in absorbance to zero. Aggregation onset occurs at 40 °C, consistent with previously discussed temperature-dependent DLS measurements. However, 0.2 mg mL^{-1} of microgel cross-linked using 5 mol% A-Phe-Phe-Me exhibited no change in CD signal intensity when subjected to a temperature increase from 25 to 65 °C, indicating the absence of aggregation (Fig. S11d–e, SI), in agreement with the DLS data (see Section 2.2).

Furthermore, the thermal effect on π-π stacking was monitored by recording temperature-dependent CD spectra. A decrease in signal intensity at 226 nm with increasing temperature was observed for microgels (0.2 mg mL^{-1}) targeting 20 mol% A-Phe-Phe-Me (Fig. S11a–b, SI). This is likely a result of microgel aggregation at elevated temperatures, as indicated by a concurrent drop in absorbance to zero. Aggregation onset occurs at 40 °C, consistent with previously discussed temperature-dependent DLS measurements. However, 0.2 mg mL^{-1} of microgel cross-linked using 5 mol% A-Phe-Phe-Me exhibited no change in CD signal intensity when subjected to a temperature increase from 25 to 65 °C, indicating the absence of aggregation (Fig. S11d–e, SI), in agreement with the DLS data (see Section 2.2).

2.5. Organic solvent-induced degradation

A degradation study with organic solvent was performed to study the stability and degradation potential of the previously characterized microgels. Therefore, the lyophilized microgels of the three systems with chemical and physical cross-links were redissolved in water and tetrahydrofuran (THF) and characterized by SEM (Fig. 6). All microgels redissolve in water with no visible aggregation, which can be seen visually from the turbid solutions as well as from the SEM images. The BIS cross-linked microgel shows no significant difference from being redissolved in THF compared to water (Fig. 6a). Measuring the diameter

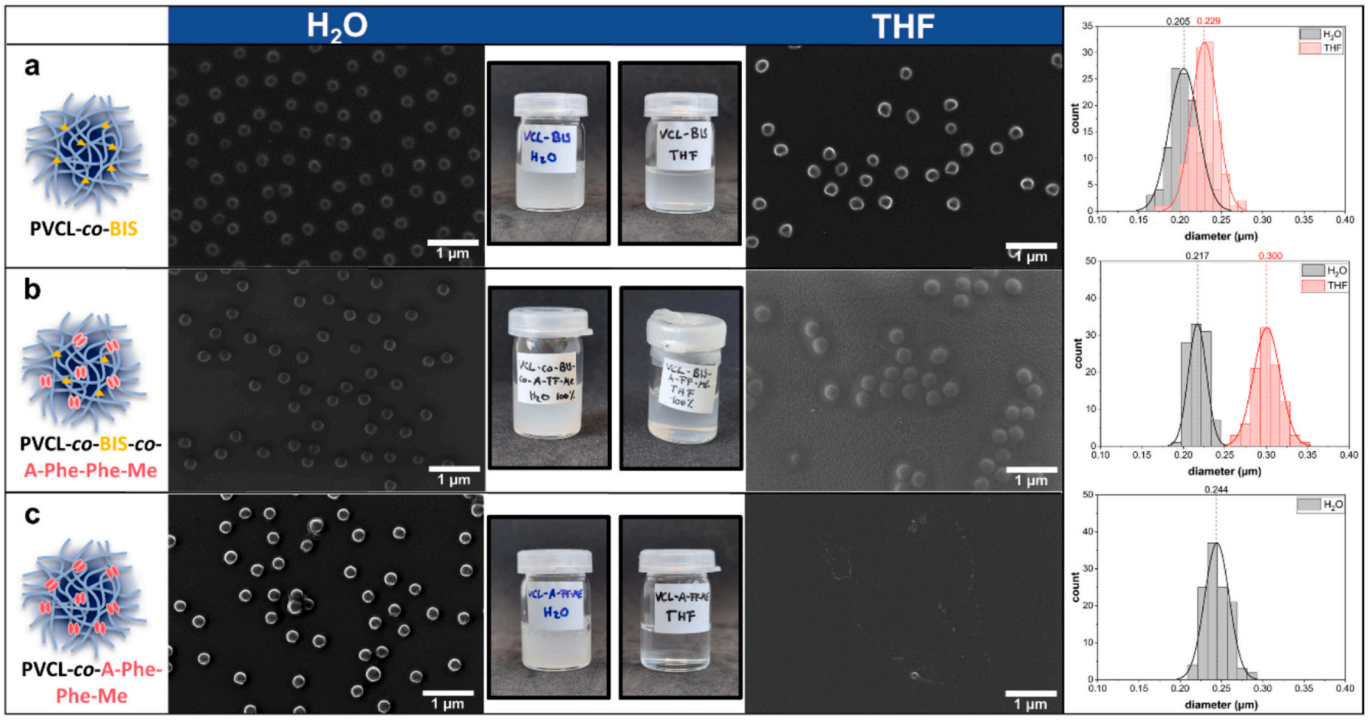

Fig. 6. Organic solvent-induced degradation of physically and chemically cross-linked microgels. SEM analysis of the three different microgel systems cross-linked by (a) only BIS, (b) a combination of BIS and A-Phe-Phe-Me, and (c) only A-Phe-Phe-Me. Each row presents the following, from left to right: a schematic representation of the microgels, an SEM image of the microgels redispersed in water from the lyophilized sample, a photograph of the reaction solution in water and THF (c = 2 mg mL^{-1}), an SEM image of the microgels redispersed in THF, and a histogram displaying the microgel diameter measured from multiple SEM images (red = in THF, black = in water). (For interpretation of the references to colour in this figure legend, the reader is referred to the web *v*ersion of this article.)

of several SEM images reveals that the microgels redispersed in THF are 229 nm on average, slightly larger than the microgels redispersed in water, with an average of 205 nm. However, the microgels consisting of chemical and physical cross-links from BIS and A-Phe-Phe-Me, respectively, have an average diameter of 300 nm when being redissolved in THF, which is 38% larger in contrast to an average diameter of 217 nm when being redispersed in water (Fig. 6b). This could be due to the breaking of the physical cross-links in THF. As a result, the microgels are only cross-linked by the remaining covalent cross-links, which makes the system more flexible, as there are fewer cross-links. The PVCL-*co*-BIS-*co*-A-Phe-Phe-Me microgels were additionally dialyzed again in water and analyzed by DLS, revealing that there is a small increase in size from 610 to 734 nm in the swollen state, as well as in the collapsed state from 370 to 439. PDI and swelling ratios are similar (Fig. S10, Table S3).

A degradation study with organic solvent was performed to study the stability and degradation potential of the previously characterized microgels. Therefore, the lyophilized microgels of the three systems with chemical and physical cross-links were redissolved in water and tetrahydrofuran (THF) and characterized by SEM (Fig. 6). All microgels redissolve in water with no visible aggregation, which can be seen visually from the turbid solutions as well as from the SEM images. The BIS cross-linked microgel shows no significant difference from being redissolved in THF compared to water (Fig. 6a). Measuring the diameter of several SEM images reveals that the microgels redispersed in THF are 229 nm on average, slightly larger than the microgels redispersed in water, with an average of 205 nm. However, the microgels consisting of chemical and physical cross-links from BIS and A-Phe-Phe-Me, respectively, have an average diameter of 300 nm when being redissolved in THF, which is 38% larger in contrast to an average diameter of 217 nm when being redispersed in water (Fig. 6b). This could be due to the breaking of the physical cross-links in THF. As a result, the microgels are only cross-linked by the remaining covalent cross-links, which makes the system more flexible, as there are fewer cross-links. The PVCL-*co*-BIS-*co*-A-Phe-Phe-Me microgels were additionally dialyzed again in water and analyzed by DLS, revealing that there is a small increase in size from 610 to 734 nm in the swollen state, as well as in the collapsed state from 370 to 439. PDI and swelling ratios are similar (Fig. S10, Table S3).

Finally, the microgel system, when cross-linked solely by the physical cross-linker, exhibited no optical turbidity upon dissolution in THF (Fig. 6c). Furthermore, no detectable particles are left in the SEM analysis, showing that the microgels fully disintegrate. The degradation product of the physically cross-linked microgels was further investigated using size exclusion chromatography (SEC). Therefore, the microgels were dissolved in DMF. In contrast to the PVCL-*co*-BIS microgels, the PVCL-*co*-A-Phe-Phe-Me microgel sample could easily be filtered through a 0.2 µm syringe filter, indicating the disassembly and absence of large, cross-linked particles. The SEC diagram shows a broad distribution with molecular weights (M_w) of 675 kDa (Fig. S13, SI).

Finally, the microgel system, when cross-linked solely by the physical cross-linker, exhibited no optical turbidity upon dissolution in THF (Fig. 6c). Furthermore, no detectable particles are left in the SEM analysis, showing that the microgels fully disintegrate. The degradation product of the physically cross-linked microgels was further investigated using size exclusion chromatography (SEC). Therefore, the microgels were dissolved in DMF. In contrast to the PVCL-*co*-BIS microgels, the PVCL-*co*-A-Phe-Phe-Me microgel sample could easily be filtered through a 0.2 µm syringe filter, indicating the disassembly and absence of large, cross-linked particles. The SEC diagram shows a broad distribution with molecular weights (M_w) of 675 kDa (Fig. S13, SI).

To further investigate the degradation by solvent, the physically cross-linked microgels were examined in different water/THF mixtures. The samples were characterized by SEM and DLS (Fig. 7). While the microgels are fully intact at 100 v% water and 0 v% THF, they gradually start to disassemble with an increasing solvent ratio. When dissolving them in a solution of 25 v% THF, small particles start to disassemble from the microgels. Overall, the majority of the microgels are still intact,

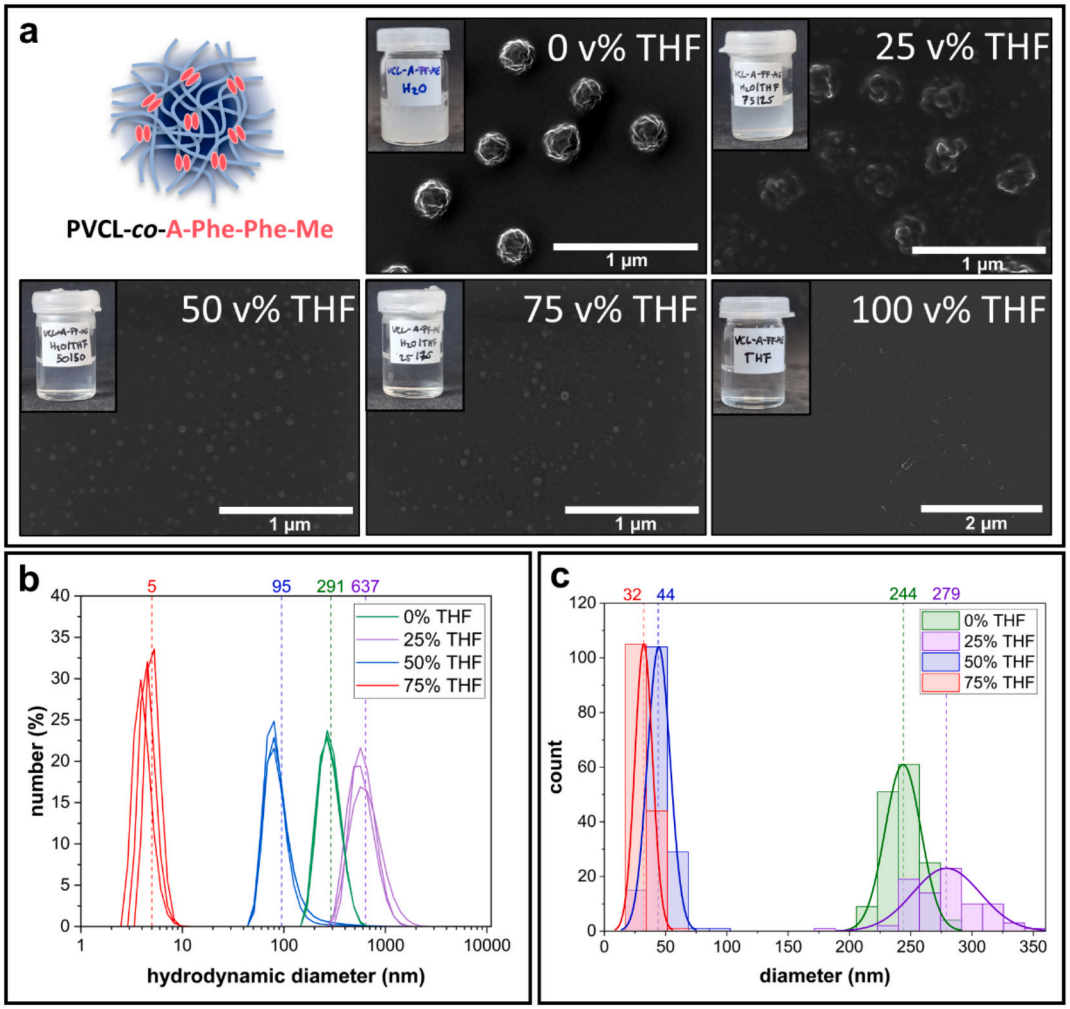

Fig. 7. Degradation of PVCL-*co*-A-Phe-Phe-Me microgels in THF with varying THF to water ratios. (a) SEM images of microgels with 5 mol% A-Phe-Phe-Me, lyophilized and redissolved in solvent mixtures between 0 and 100 v% THF. Inserted is a picture of the respective solvent solution (c = 2 mg mL^{-1}). (b) Size distribution of microgels between 0 and 75 v% THF by number measured by DLS at 50 °C. (c) Histograms illustrating the diameters of the particles measured from SEM images between 0 and 75 v% THF.

however, the roughness of the surface increases. At a volume ratio of 50 v% THF, the large microgels are fully disassembled into small particles. The size decreases further with 75 v% THF, while at 100 v% THF, no particles and only polymer traces could be detected in SEM images (Fig. 7a). The microgel sizes were measured from several SEM images and are depicted as a histogram in Fig. 7c.

This behavior is challenging to analyze using DLS, as particle disassembly increases polydispersity and can lead to aggregate formation. To better capture the disassembly process, size distribution by number was chosen over size distribution by intensity, as it provides a more accurate representation of polydisperse systems and emphasizes smaller particles [62,63]. The size distribution by number shows the same trend as that observed in SEM. The particle size increases for the sample dissolved in 25 v% THF compared to the one with 0 v% THF, while with increasing THF ratios of 50 and 75, the particles become significantly smaller (Fig. 7b). In agreement with the SEM and DLS results, there is a decrease in turbidity visually detectable with increasing THF ratio when comparing the solutions depicted in the inserted images in Fig. 7a, which is not observed for the microgels containing chemical cross-links (Fig. S12, SI).

This behavior is challenging to analyze using DLS, as particle disassembly increases polydispersity and can lead to aggregate formation. To better capture the disassembly process, size distribution by number was chosen over size distribution by intensity, as it provides a more accurate representation of polydisperse systems and emphasizes smaller particles [62,63]. The size distribution by number shows the same trend as that observed in SEM. The particle size increases for the sample dissolved in 25 v% THF compared to the one with 0 v% THF, while with increasing THF ratios of 50 and 75, the particles become significantly smaller (Fig. 7b). In agreement with the SEM and DLS results, there is a decrease in turbidity visually detectable with increasing THF ratio when comparing the solutions depicted in the inserted images in Fig. 7a, which is not observed for the microgels containing chemical cross-links (Fig. S12, SI).

2.6. *Concentration-dependent microgel morphology*

Concentration plays a critical role in self-assembling processes. Literature reports indicate that the self-assembly of Phe-Phe-based nanostructures depends on the peptide concentration, enabling, for example, structural variations from nanotubes to nanovesicles as peptide concentration decreases [34,64]. Inspired by these results, the formation of A-Phe-Phe-Me cross-linked microgels was further examined in terms of their concentration during synthesis. This approach could offer a promising strategy for tailoring microgel morphology, particularly for the fabrication of asymmetric-shaped microgels, which are challenging to achieve via precipitation polymerization. Therefore, the synthesis was performed with a constant total monomer amount of 1.6 mmol and a

fixed monomer ratio of 95 to 5 (VCL to A-Phe-Phe-Me) while varying the reaction volume between 20 mL and 10 mL. The solvent ratio of 90 to 10 (Water to DMSO) as well as the absolute amount of initiator was kept constant for each synthesis. The microgels were characterized by SEM and DLS (Fig. 8). Increasing the monomer concentration by decreasing the volume showed two effects on the microgels. Firstly, according to DLS measurements, the $D_{h,20^\circ C}$ of these microgels increases from 649 to 1170 nm when changing from a total volume of 20 mL to 15 mL. The size increases further to 1940 nm for a volume of 10 mL. The $D_{h,50^\circ C}$, also increases from 292 to 385 to 508 nm (Fig. 8d). The rise in size is accompanied by an increase in PDI and, therefore, a decrease in monodispersity. Secondly, a change in morphology is visible in the SEM images. While the microgels prepared in 20 mL reaction volume are highly monodisperse and spherical, the decrease in volume results not only in a size increase but also in the formation of dimers and trimers (Fig. 8a-c). Therefore, the reduction in reaction volume results in an increase in non-spherical, partly asymmetric-shaped microgels, which could be due to increased dipeptide concentration as well as the increased initiator concentration.

The decrease in reaction volume also affects the incorporation efficiency of A-Phe-Phe-Me, which decreases from 4.2 to 3.5 to 3.0 mol% for the respective volumes (Table S1, SI). This can be attributed to the overall lower amount of DMSO at reduced volumes, as discussed in Section 2.1. However, the total yield remains unaffected by the change in volume.

The decrease in reaction volume also affects the incorporation efficiency of A-Phe-Phe-Me, which decreases from 4.2 to 3.5 to 3.0 mol% for the respective volumes (Table S1, SI). This can be attributed to the overall lower amount of DMSO at reduced volumes, as discussed in Section 2.1. However, the total yield remains unaffected by the change in volume.

3. Conclusions

In this study, we successfully synthesized and characterized novel poly(*N*-vinylcaprolactam) (PVCL) based microgels containing supramolecular cross-links originating from a diphenylalanine-based monomer bearing the well-known *L*-phenylalanyl-*L*-phenylalanine (Phe-Phe) motif. The monomer was synthesized and copolymerized with VCL via precipitation polymerization, leading to supramolecular cross-linking involving hydrogen bonds and aromatic interactions. The chemical structures and compositions of the monomer and microgels were validated using ^{1}H NMR, FTIR, and Raman spectroscopy, confirming the efficient incorporation of the dipeptide. It was shown that the microgel formation is driven by π-π stacking using CD spectroscopy. A detailed analysis of the thermoresponsive behavior through DLS showed that the physical cross-linked microgels are comparable to the chemical cross-linked ones. However, small physically cross-linked microgels as well as microgels with high physical cross-linker content showed a pronounced tendency to form aggregates at temperatures above 40 °C. The data suggest that the heat-induced aggregation is facilitated by the combined effect of the hydrophobic A-Phe-Phe-Me moiety and the underlying structural differences in the swelling ratio SR. We therefore hypothesize that the non-covalent interactions of the Phe-Phe motif are not only limited to generating intramolecular cross-links in the microgels but could open the possibility for the preparation of microgel assemblies. The microgels were further examined regarding their degradation potential by SEM and DLS. In this model study, the physical cross-links were broken using organic solvents, potentially allowing for the controlled release and delivery of biomacromolecules. Lastly, the morphology of the microgels can be tuned by the reaction solution concentration during synthesis. This opens the possibility for the formation of asymmetric-shaped microgels, which are challenging to produce using precipitation polymerization. These findings contribute to a deeper understanding of microgel formation, aggregate formation, degradation, and morphology changes using physical cross-links. Compared to previous studies on supramolecular cross-linked microgels, which are mostly based on host-guest interactions or metal complexation, our work demonstrates a novel, simple approach to apply physical cross-linking via π-π-stacking by short aromatic peptides, making the microgels interesting candidates for applications in the biomedical field, where controlled degradation and stimuli-responsiveness are critical factors. In future work, employing feeding strategies during microgel formation could effectively control the Phe-Phe unit distribution. Specifically, generating surface-bound Phe-Phe groups would be beneficial for the supramolecular assembly of microgels, which is currently often achieved using host-guest interactions, electrostatic interactions, or metal coordination [65].

4. Experimental section

4.1. Materials

N-vinylcaprolactam (VCL, 98%, Sigma-Aldrich) was purified by distillation under vacuum and recrystallization from *n*-hexane before usage. All of the following chemicals were used as received. *N,N′*-methylenbis(acrylamide) (BIS, 99%), 2,2–azobis(*N*-methylpropionamidine) dihydrochloride (AMPA, 97%), acryloyl chloride (97%), 4-(dimethylamino)pyridine (DMAP, 99%), and magnesium sulfate ($MgSO_4$, 98%) were purchased from Sigma-Aldrich. *L*-phenylalanyl-*L*-phenylalanine (98%, Phe-Phe) and acetyl chloride (98%) were purchased from TCI. Furthermore, triethylamine (TEA, 99%) and cetyltrimethylammonium bromide (CTAB, 99%) were purchased from Alfa Aesar and Carl Roth, respectively. Anhydrous methanol (99.8%, Sigma-Aldrich), anhydrous dichloromethane (DCM, 99.8%, Sigma-Aldrich), and dimethylsulfoxide (DMSO, 99.9%, Fisher Chemical) were used as solvents during synthesis. For analysis purposes, tetrahydrofuran (THF, 99.9%, Sigma Aldrich), deuterated chloroform ($CDCl_3$, 99.8%, Deutero), dimethyl sulfoxide (DMSO-d_6, 99.8%, Deutero) with dimethyl terephthalate (DMT, certified reference material, standard for quantitative NMR, Sigma-Aldrich), and *N,N*-dimethylformamide (DMF, 99.8, Sigma-Aldrich) were used.

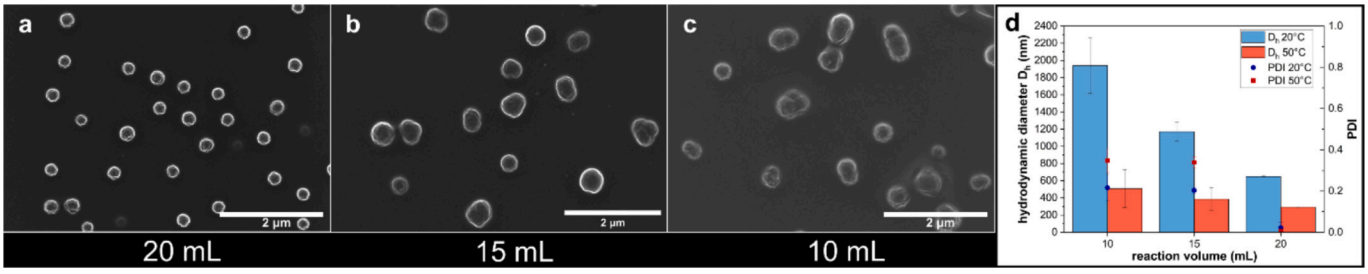

Fig. 8. Concentration-dependent morphological changes in A-Phe-Phe-Me cross-linked microgels. (a-c) SEM images of microgels prepared using 20, 15, and 10 mL of total reaction volume. (d) Hydrodynamic diameters and PDIs of microgels measured at 20 and 50 °C. Each value represents the average of at least four replicate measurements.

4.1.1. Monomer synthesis

The monomer *N*-acryloyl-*L*-phenylalanyl-*L*-phenylalanine methyl ester (A-Phe-Phe-Me) was synthesized in two steps via esterification of Phe-Phe followed by an acryloyl substitution as reported previously [48,50]. In the first step, Phe-Phe (0.99993 g, 3.20 mmol) was dissolved in anhydrous methanol (50 mL). The mixture was maintained in an ice bath while acetyl chloride (5 mL, 70.07 mmol) was added dropwise. The resulting solution was stirred at 0 °C for 2 h, followed by stirring at room temperature overnight. The solvent was removed under reduced pressure, yielding the white solid *L*-phenylalanyl-*L*-phenylalanine methyl ester (Phe-Phe-Me, 1.07082 g, 2.95 mmol, 92.2%). For the second step, Phe-Phe-Me (0.9764 g, 2.69 mmol) was dissolved in anhydrous DCM (40 mL), followed by the addition of TEA (804 µL, 5.77 mmol) and DMAP (36.2 mg, 0.296 mmol). Acryloyl chloride (370 µL, 4.55 mmol) in DCM (5 mL) was added over 15 min while stirring the solution in an ice bath. The solution was stirred at room temperature overnight, diluted with DCM (40 mL), and washed with HCl (1 M, 85 mL) and brine (85 mL). The organic phase was dried over $MgSO_4$ and the solvent was removed under reduced pressure. The obtained product was recrystallized from DCM at −18 °C, filtered, and dried under vacuum to obtain the white solid A-Phe-Phe-Me (0.37339 g, 0.981 mmol, 36.5%). The final product was analyzed by ^{1}H NMR spectroscopy (Fig. S3, SI).

The monomer *N*-acryloyl-*L*-phenylalanyl-*L*-phenylalanine methyl ester (A-Phe-Phe-Me) was synthesized in two steps via esterification of Phe-Phe followed by an acryloyl substitution as reported previously [48,50]. In the first step, Phe-Phe (0.99993 g, 3.20 mmol) was dissolved in anhydrous methanol (50 mL). The mixture was maintained in an ice bath while acetyl chloride (5 mL, 70.07 mmol) was added dropwise. The resulting solution was stirred at 0 °C for 2 h, followed by stirring at room temperature overnight. The solvent was removed under reduced pressure, yielding the white solid *L*-phenylalanyl-*L*-phenylalanine methyl ester (Phe-Phe-Me, 1.07082 g, 2.95 mmol, 92.2%). For the second step, Phe-Phe-Me (0.9764 g, 2.69 mmol) was dissolved in anhydrous DCM (40 mL), followed by the addition of TEA (804 µL, 5.77 mmol) and DMAP (36.2 mg, 0.296 mmol). Acryloyl chloride (370 µL, 4.55 mmol) in DCM (5 mL) was added over 15 min while stirring the solution in an ice bath. The solution was stirred at room temperature overnight, diluted with DCM (40 mL), and washed with HCl (1 M, 85 mL) and brine (85 mL). The organic phase was dried over $MgSO_4$ and the solvent was removed under reduced pressure. The obtained product was recrystallized from DCM at −18 °C, filtered, and dried under vacuum to obtain the white solid A-Phe-Phe-Me (0.37339 g, 0.981 mmol, 36.5%). The final product was analyzed by ^{1}H NMR spectroscopy (Fig. S3, SI).

4.1.2. Microgel synthesis

The microgels were synthesized using precipitation polymerization. The following procedure is exemplary for a synthesis using 5 mol% A-Phe-Phe-Me and 10 v% DMSO. VCL (1.57 mmol) was dissolved in ultrapure water and purged with nitrogen for 30 min while heating to 70 °C. AMPA (0.0032 mmol) and A-Phe-Phe-Me (0.08 mmol) were dissolved in ultrapure water (18 mL) and DMSO (2 mL), respectively, and purged with nitrogen for 20 min. The reaction was started by adding the AMPA solution, which was directly followed by A-Phe-Phe-Me addition. The reaction mixture was stirred at 70 °C for 3 h before being cooled to room temperature and stirred overnight. Low molecular weight impurities were removed by dialysis using a tube with a molecular weight cut-off of 12–14 kD in deionized water for 7 days, changing the water 3 times a day. Parts of the microgel solution were lyophilized to determine the yield and perform further characterization. For the concentration-dependent synthesis, the total volume of the reaction was adjusted to 15 and 10 mL. The absolute amounts of *V*CL, A-Phe-Phe-Me, and AMPA were held constant, and the water to DMSO ratio remained at 90:10.

4.1.3. Centrifugation experiments

To investigate the amount of higher molecular weight species remaining in the microgel dispersion, centrifugation was applied. For the high-speed centrifugation, an Eppendorf 5418R centrifuge was used, applying the maximal relative centrifugal force (RCF) of 16.800 x g for 30 min at 20 °C. For the ultracentrifugation, an Optima centrifuge from Beckman was used, applying 80.000 x g for 80 min at 4 °C. For both centrifugation experiments, 1.0–1.5 mL of the dialyzed samples containing 5 and 20 mol% A-Phe-Phe-Me was used. 1.0–1.2 mL of the supernatant was collected without destroying the pellet and lyophilized. The polymer mass was determined gravimetrically.

4.1.4. Dynamic light scattering

Dynamic light scattering (DLS) was performed to determine the hydrodynamic diameter and the size distribution of the microgels using a Zetasizer Ultra by Malvern Panalytical and analyzed using the software ZS Xplorer. To avoid particle-particle interactions and the confounding effects of multiple scattering, purified microgels were dispersed in ultrapure water. A typical low concentration of 0.01–0.1 mg mL^{-1} was used, which yielded minimal turbidity (mean count rates between 200 and 600). The samples were transferred into a disposable capillary cell of the type DTS0012. A glass cuvette was used in the case where THF and mixtures of THF/water were used for the dilution at concentrations between 0.2 and 0.3 mg mL^{-1}. The samples were measured at a fixed scattering angle of 90° (side scatter) and a laser beam operating at λ = 632.8 nm at temperatures of 20 and 50 °C. Each reported value is the average of at least four independent consecutive runs, starting with the lower temperature. After reaching a stable temperature, the samples were allowed to equilibrate for an additional 60 s at 20 °C and 120 s at 50 °C. For the temperature-dependent measurements, the temperature was set from 5 to 67 °C (and backward), measured in 1 °C steps with an equilibration time of 120 s at each temperature. Each reported value is the average of at least three independent consecutive runs. The mean peak values from the intensity-weighted or number-weighted distributions were used for the size determination.

4.1.5. Zeta potential measurements

The zeta potential (ζ) was measured with a Zetasizer Ultra (Malvern Panalytical, Germany) and a disposable capillary cell (DTS1070, Malvern Panalytical). For all measurements, the sample was diluted with ultrapure water to concentrations of 0.2 mg mL^{-1}. The dispersions were measured at 20 and 55 °C with an applied voltage of 150 V. Each reported value is the average of at least four independent consecutive runs, starting with the lower temperature. After reaching a stable temperature, the samples were allowed to equilibrate for an additional 120 s at 20 °C and 600 s at 55 °C. The software ZS Xplorer was used to analyze the results.

4.1.6. Scanning and transmission electron microscopy

For scanning electron and scanning transmission electron microscopy (SEM/STEM) measurements, an ultra-high-resolution SU-9000 microscope by Hitachi was used. The electron energy was set to 30 kV, and the magnification was between x20000 and x100000. The scanning electron (SE) and bright-field STEM (BF-STEM) modes were applied. Samples were diluted with HPLC-grade water or THF to a concentration of 0.8 mg mL^{-1}, which was determined by the lyophilization of a known volume. A droplet of 7 µL was placed onto a carbon-coated copper grid (400 Mesh), while a filter paper absorbed the excess liquid. The sample was set to dry for several hours so that the solvent could evaporate before the measurement.

4.1.7. Nuclear magnetic resonance spectroscopy

^{1}H NMR spectroscopy of the monomer and microgels was recorded on a Bruker AV400 Spectrometer at 400 MHz. For all measurements, deuterated DMSO (DMSO-d_6, chemical shift δ H = 2.50 ppm, water residue chemical shift δ H = 3.30 ppm) or deuterated chloroform ($CDCl_3$, chemical shift δ H = 7.26 ppm) were used as a solvent. Dimethyl terephthalate (DMT) was used as an internal standard in DMSO-d_6 for

quantitative NMR measurements. The NMR spectra, as well as the calculations for the quantitative determination, can be found in the SI.

^{1}H NMR spectroscopy of the monomer and microgels was recorded on a Bruker A*V*400 Spectrometer at 400 MHz. For all measurements, deuterated DMSO (DMSO-d_6, chemical shift δ H = 2.50 ppm, water residue chemical shift δ H = 3.30 ppm) or deuterated chloroform ($CDCl_3$, chemical shift δ H = 7.26 ppm) were used as a solvent. Dimethyl terephthalate (DMT) was used as an internal standard in DMSO-d_6 for quantitative NMR measurements. The NMR spectra, as well as the calculations for the quantitative determination, can be found in the SI.

4.1.8. Circular dichroism spectroscopy

Circular dichroism (CD) spectra of the microgels were recorded on a JASCO J-1500 Spectrometer using a 1 mm path-length quartz cuvette. Each spectrum is an average of three accumulations. The spectral contributions from the water were subtracted. The spectra were recorded using the following parameters: 200–300 nm wavelength range, 1 nm data pitch, 1 nm bandwidth, 0.5 s response, and 100 nm min^{-1} of scanning speed. The microgels were diluted with HPLC-grade water to concentrations between 0.01 and 0.5 mg mL^{-1}.

4.1.9. Gel permeation chromatography (GPC)

Gel permeation chromatography (GPC), utilizing size exclusion chromatography (SEC), was employed to determine the average molecular weights (M_w, M_n) and molecular weight distributions (M_w/M_n) of the disassembled PVCL-*co*-A-Phe-Phe-Me microgel. Dimethylformamide (DMF) was used as the eluent with 1 g L^{-1} Lithium Bromide, and SEC was performed with a Bischoff HPLC compact pump coupled to a Jasco RI-2031 plus refractive index detector. Three columns containing SS GRAM gel were used for separation. Data analysis was conducted using PSS WinGPC UniChrom software. For the measurements, lyophilized microgels were dissolved in the eluent with a concentration of 7 mg mL^{-1} and filtered through a syringe filter with a pore size of 0.2 µm.

4.1.10. Fourier transform infrared and Raman spectroscopy

To investigate the microgel and monomer structure, Fourier transform infrared (FTIR) spectra were recorded using a PerkinElmer FTIR spectrometer. Measurements were taken between 400 and 4000 cm^{-1} with a resolution of 4 cm^{-1} and 4 scans per measurement. The data was analyzed using the Spectrum IR software (version 10.7.2). Raman spectroscopy was employed using a Bruker RFS 100/S Raman spectrometer equipped with a Nd:YAG laser (k = 1064 nm). The measurements were conducted with a spectral resolution of 4 cm^{-1}, power of 200 mW, and 1000 scans. For the measurements, the lyophilized microgels were compressed into an aluminum pan. For the data analysis, the software OPUS 4.0 was used. Baseline corrections were performed.

4.1.11. Atomic force microscopy

Atomic force microscopy (AFM) images were recorded using a NanoScope V from Veeco Instruments in tapping mode. As a cantilever, an NCH-50 POINTPROBE®-Silicon SPM-Sensor from Nanoworld with a resonance frequency of 320 kHz and a force constant of 42 Nm^{-1} was used. The samples (50 µL, 5 mg mL^{-1}) were spin-coated on a silicon wafer using a WS-650SZ-6NPP/LITE spin-coater by Laurell, applying 2000 rpm. The wafers were plasma treated at 0.2 mbar for 60 s beforehand using a Flecro 10USB-MFC plasma oven by Plasma Technology. The recorded images were analyzed with the software Gwyddion.

CRediT authorship contribution statement

Nadja A. Wolter: Writing – review & editing, Writing – original draft, Visualization, Methodology, Investigation, Formal analysis, Conceptualization. **Gurudas Chakraborty:** Writing – review & editing, Methodology, Investigation, Formal analysis. **Hannah Küttner:** Writing – review & editing, Investigation. **Andreas Herrmann:** Writing – review & editing, Funding acquisition. **Andrij Pich:** Writing – review & editing, Supervision, Funding acquisition, Conceptualization.

Declaration of competing interest

The authors declare that they have no known competing financial interests or personal relationships that could have appeared to influence the work reported in this paper.

Acknowledgments

This work was performed as part of project B4 of the collaborative research center CRC 985 “Functional Microgels and Microgel Systems” (project number: 191948804) funded by Deutsche Forschungsgemeinschaft (DFG). The authors gratefully acknowledge Stefan Hauk for recording SEM and STEM images and Peter Koch for recording AFM images. The authors further thank the students Hanna Vander, Sitong Liu, and Marc Meyer for performing parts of the synthesis.

Declaration of generative AI in scientific writing

During the revision of this work, the authors used ChatGPT and Grammarly in order to improve the readability and language of the manuscript. After using this tool, the authors reviewed and edited the content as needed and take full responsibility for the content of the published article.

Appendix A. Supplementary data

Supplementary data to this article can be found online at https://doi.org/10.1016/j.jcis.2025.139770.

Data availability

Data will be made available on request.

References

[1] G.M. Whitesides, M. Boncheva, Beyond molecules: self-assembly of mesoscopic and macroscopic components, Proc. Natl. Acad. Sci. USA 99 (2002) 4769–4774.
[2] G.M. Whitesides, J.P. Mathias, C.T. Seto, Molecular self-assembly and Nanochemistry: a chemical strategy for the synthesis of nanostructures, Science 254 (1991) (1979) 1312–1319.
[3] G.M. Whitesides, B. Grzybowski, Self-assembly at all scales, Science 295 (2002) (1979) 2418–2421.
[4] A.C. Mendes, E.T. Baran, R.L. Reis, H.S. Azevedo, Self-assembly in nature: using the principles of nature to create complex nanobiomaterials, WIREs Nanomed. Nanobiotechnol. 5 (2013) 582–612.
[5] A. Pich, W. Richtering, Chemical Design of Responsive Microgels, Springer, Berlin, Heidelberg, 2010.
[6] F.A. Plamper, W. Richtering, Functional microgels and microgel systems, Acc. Chem. Res. 50 (2017) 131–140.
[7] R. Pelton, Temperature-sensitive aqueous microgels, Adv. Colloid Interf. Sci. 85 (2000) 1–33.
[8] S. Zhou, B. Chu, Synthesis and volume phase transition of poly(methacrylic acid-co-N-isopropylacrylamide) microgel particles in water, J. Phys. Chem. B 102 (1998) 1364–1371.
[9] T. Hoare, R. Pelton, Highly pH and temperature responsive microgels functionalized with Vinylacetic acid, Macromolecules 37 (2004) 2544–2550.
[10] D. Duracher, F. Sauzedde, A. Elaïssari, C. Pichot, L. Nabzar, Cationic amino-containing N-isopropyl-acrylamide-styrene copolymer particles: 2-surface and colloidal characteristics, Colloid Polym. Sci. 276 (1998) 920–929.
[11] M. Bekir, J. Jelken, S.H. Jung, A. Pich, C. Pacholski, A. Kopyshev, S. Santer, Dual responsiveness of microgels induced by single light stimulus, Appl. Phys. Lett. 118 (2021) 91603.
[12] Y. Lu, S. Proch, M. Schrinner, M. Drechsler, R. Kempe, M. Ballauff, Thermosensitive core-shell microgel as a “nanoreactor” for catalytic active metal nanoparticles, J. Mater. Chem. 19 (2009) 3955–3961.
[13] V.C. Lopez, J. Hadgraft, M.J. Snowden, The use of colloidal microgels as a (trans) dermal drug delivery system, Int. J. Pharm. 292 (2005) 137–147.
[14] R.H. Pelton, P. Chibante, Preparation of aqueous latices with N-isopropylacrylamide, Colloids Surf. 20 (1986) 247–256.
[15] A. Laukkanen, S.K. Wiedmer, S. Varjo, M.L. Riekkola, H. Tenhu, Stability and thermosensitive properties of various poly (N-vinylcaprolactam) microgels, Colloid Polym. Sci. 280 (2002) 65–70.

[16] H. Vihola, A. Laukkanen, L. Valtola, H. Tenhu, J. Hirvonen, Cytotoxicity of thermosensitive polymers poly(N-isopropylacrylamide), poly(N-vinylcaprolactam) and amphiphilically modified poly(N-vinylcaprolactam), Biomaterials 26 (2005) 3055–3064.
[17] S. Bernhard, M.W. Tibbitt, Supramolecular engineering of hydrogels for drug delivery, Adv. Drug Deliv. Rev. 171 (2021) 240–256.
[18] S.H. Jung, S. Schneider, F. Plamper, A. Pich, Responsive supramolecular microgels with redox-triggered cleavable crosslinks, Macromolecules 53 (2020) 1043–1053.
[19] C. Molano López, A. Pich, Supramolecular stimuli-responsive microgels crosslinked by tannic acid, Macromol. Rapid Commun. 39 (2018) 1700808.
[20] Y. Yin, S. Jiao, R. Zhang, X. Hu, Z. Shi, Z. Huang, Construction of a smart microgel glutathione peroxidase mimic based on supramolecular self-assembly, Soft Matter 11 (2015) 5301–5312.
[21] G. Kamaraju, J. Karl, S. Bulut, M. Pieper, N. Hazra, G. Chakraborty, A. Boes, A. Herrmann, U. Schwaneberg, A. Pich, Hybrid pectin-fibroin microgels with supramolecular and covalent cross-links, Biomacromolecules 26 (2025) 2331–2343.
[22] W. Liang, C.G. Lopez, W. Richtering, D. Wöll, Photo- and thermo-responsive microgels with supramolecular crosslinks for wavelength tunability of the volume phase transition temperature, Phys. Chem. Chem. Phys. 24 (2022) 14408–14415.
[23] Y. Chen, N. Ballard, S.A.F. Bon, Waterborne polymer nanogels non-covalently crosslinked by multiple hydrogen bond arrays, Polym. Chem. 4 (2012) 387–392.
[24] J. Es Sayed, C. Lorthioir, P. Banet, P. Perrin, N. Sanson, Reversible assembly of microgels by Metallo-supramolecular chemistry, Angew. Chem. Int. Ed. 59 (2020) 7042–7048.
[25] I. Antoniuk, D. Kaczmarek, A. Kardos, I. Varga, C. Amiel, Supramolecular Hydrogel Based on pNIPAm Microgels Connected via Host–Guest Interactions, Polymers (Basel) 10 (2018) 566.
[26] X. Zhao, F. Pan, H. Xu, M. Yaseen, H. Shan, C.A.E. Hauser, S. Zhang, J.R. Lu, Molecular self-assembly and applications of designer peptide amphiphiles, Chem. Soc. Rev. 39 (2010) 3480–3498.
[27] S. Fleming, R.V. Ulijn, Design of nanostructures based on aromatic peptide amphiphiles, Chem. Soc. Rev. 43 (2014) 8150–8177.
[28] X. Yan, P. Zhu, J. Li, Self-assembly and application of diphenylalanine-based nanostructures, Chem. Soc. Rev. 39 (2010) 1877–1890.
[29] L. Adler-Abramovich, E. Gazit, The physical properties of supramolecular peptide assemblies: from building block association to technological applications, Chem. Soc. Rev. 43 (2014) 6881–6893.
[30] A. Levin, T.A. Hakala, L. Schnaider, G.J.L. Bernardes, E. Gazit, T.P.J. Knowles, Biomimetic peptide self-assembly for functional materials, Nat. Rev. Chem. 4 (2020) 615–634.
[31] M. Reches, E. Gazit, Designed aromatic homo-dipeptides: formation of ordered nanostructures and potential nanotechnological applications, Phys. Biol. 3 (2006) S10–S19.
[32] M. Reches, E. Gazit, Self-assembly of peptide nanotubes and amyloid-like structures by charged-termini-capped diphenylalanine peptide analogues, Isr. J. Chem. 45 (2005) 363–371.
[33] J. Wang, K. Liu, L. Yan, A. Wang, S. Bai, X. Yan, Trace solvent as a predominant factor to tune dipeptide self-assembly, ACS Nano 10 (2016) 2138–2143.
[34] C. Guo, Y. Luo, R. Zhou, G. Wei, Probing the self-assembly mechanism of diphenylalanine-based peptide nanovesicles and nanotubes, ACS Nano 6 (2012) 3907–3918.
[35] P. Kumaraswamy, R. Lakshmanan, S. Sethuraman, U.M. Krishnan, Self-assembly of peptides: influence of substrate, pH and medium on the formation of supramolecular assemblies, Soft Matter 7 (2011) 2744–2754.
[36] L. Adler-Abramovich, D. Aronov, P. Beker, M. Yevnin, S. Stempler, L. Buzhansky, G. Rosenman, E. Gazit, Self-assembled arrays of peptide nanotubes by vapour deposition, Nat. Nanotechnol. 4 (2009) 849–854.
[37] V. Nguyen, R. Zhu, K. Jenkins, R. Yang, Self-assembly of diphenylalanine peptide with controlled polarization for power generation, Nat. Commun. 7 (2016) 13566.
[38] J.H. Kim, J. Ryu, C.B. Park, Selective detection of neurotoxin by photoluminescent peptide nanotubes, Small 7 (2011) 718–722.
[39] J.H. Kim, S.Y. Lim, D.H. Nam, J. Ryu, S.H. Ku, C.B. Park, Self-assembled, photoluminescent peptide hydrogel as a versatile platform for enzyme-based optical biosensors, Biosens. Bioelectron. 26 (2011) 1860–1865.
[40] M. Zhou, A.M. Smith, A.K. Das, N.W. Hodson, R.F. Collins, R.V. Ulijn, J.E. Gough, Self-assembled peptide-based hydrogels as scaffolds for anchorage-dependent cells, Biomaterials 30 (2009) 2523–2530.
[41] Y. Hu, H. Shi, X. Ma, T. Xia, Y. Wu, L. Chen, Z. Ren, L. Lei, J. Jiang, J. Wang, X. Li, Highly stable fibronectin-mimetic-peptide-based supramolecular hydrogel to accelerate corneal wound healing, Acta Biomater. 159 (2023) 128–139.
[42] R. Ischakov, L. Adler-Abramovich, L. Buzhansky, T. Shekhter, E. Gazit, Peptide-based hydrogel nanoparticles as effective drug delivery agents, Bioorg. Med. Chem. 21 (2013) 3517–3522.
[43] H. Liu, X. Bi, Y. Wu, M. Pan, X. Ma, L. Mo, J. Wang, X. Li, Cationic self-assembled peptide-based molecular hydrogels for extended ocular drug delivery, Acta Biomater. 131 (2021) 162–171.
[44] R.F. Silva, D.R. Araújo, E.R. Silva, R.A. Ando, W.A. Alves, L -diphenylalanine microtubes as a potential drug-delivery system: characterization, release kinetics, and cytotoxicity, Langmuir 29 (2013) 10205–10212.
[45] H. Skaat, R. Chen, I. Grinberg, S. Margel, Engineered polymer nanoparticles containing hydrophobic dipeptide for inhibition of amyloid-β fibrillation, Biomacromolecules 13 (2012) 2662–2670.
[46] C.-J. Kim, J. Park, X. Hu, S.K. Albert, S.-J. Park, Peptide-driven shape control of low-dimensional DNA nanostructures, ACS Nano 14 (2020) 2276–2284.
[47] R. Yonenuma, A. Ishizuki, K. Nakabayashi, H. Mori, Synthesis and hierarchical self-assembly of diphenylalanine-based homopolymer and copolymers by RAFT polymerization, J. Polym. Sci. Part A Polym. Chem. 57 (2019) 2562–2574.
[48] O. Melamed, S. Margel, Poly(N-vinyl α-amino acid) microspheres: a model—poly (N-vinyl α-phenyl alanine) microspheres: synthesis and characterization, Colloids Surf. A Physicochem. Eng. Asp. 208 (2002) 147–157.
[49] J.L. Warren, P.A. Dykeman-Bermingham, A.S. Knight, Controlling amphiphilic polymer folding beyond the primary structure with protein-mimetic Di (phenylalanine), J. Am. Chem. Soc. 143 (2021) 13228–13234.
[50] A. Nudelman, Y. Bechor, E. Falb, B. Fischer, B.A. Wexler, A. Nudelman, Acetyl chloride-methanol as a convenient reagent for: (A) quantitative formation of amine hydrochlorides (B) carboxylate Ester formation (C) mild removal of N-t-Boc-protective group, Synth. Commun. 28 (1998) 471–474.
[51] W. McPhee, K.C. Tam, R. Pelton, Poly(N-isopropylacrylamide) latices prepared with sodium dodecyl Sulfate, J. Colloid Interface Sci. 156 (1993) 24–30.
[52] M. Brugnoni, A.C. Nickel, L.C. Kröger, A. Scotti, A. Pich, K. Leonhard, W. Richtering, Synthesis and structure of deuterated ultra-low cross-linked poly(N -isopropylacrylamide) microgels, Polym. Chem. 10 (2019) 2397–2405.
[53] N.A. Wolter, H. Küttner, J. Schmitz, M. Karg, A. Pich, Asymmetric microgels with Tunable morphologies by assembly-guided polymerization of liquid crystalline monomers, Small 21 (2025) 2410502.
[54] S.D. Fried, S. Bagchi, S.G. Boxer, Measuring electrostatic fields in both hydrogen-bonding and non-hydrogen-bonding environments using carbonyl vibrational probes, J. Am. Chem. Soc. 135 (2013) 11181–11192.
[55] A. Balaceanu, D.E. Demco, M. Möller, A. Pich, Microgel heterogeneous morphology reflected in temperature-induced volume transition and 1 H high-resolution transverse relaxation NMR. The case of poly(N-vinylcaprolactam) microgel, Macromolecules 44 (2011) 2161–2169.
[56] F. Schneider, A. Balaceanu, A. Feoktystov, V. Pipich, Y. Wu, J. Rgen Allgaier, W. Pyckhout-Hintzen, A. Pich, G.J. Schneider, Monitoring the internal structure of poly(N-vinylcaprolactam) microgels with variable cross-link concentration, Langmuir 30 (2014) 15317–15326.
[57] Y. Utashiro, M. Takiguchi, M. Satoh, Zeta potential of PNIPAM microgel particles dispersed in water—effects of charged radical initiators vs. OH− ion adsorption, Colloid Polym. Sci. 295 (2017) 45–52.
[58] A. Imaz, J. Forcada, N-vinylcaprolactam-based microgels: synthesis and characterization, J. Polym. Sci. A Polym. Chem. 46 (2008) 2510–2524.
[59] V. Castelletto, I.W. Hamley, Self assembly of a model amphiphilic phenylalanine peptide/polyethylene glycol block copolymer in aqueous solution, Biophys. Chem. 141 (2009) 169–174.
[60] C. Diaferia, C. Avitabile, M. Leone, E. Gallo, M. Saviano, A. Accardo, A. Romanelli, Diphenylalanine motif drives self-assembling in hybrid PNA-peptide conjugates, Chem. Eur. J. 27 (2021) 14307–14316.
[61] S. Marchesan, L. Waddington, C.D. Easton, D.A. Winkler, L. Goodall, J. Forsythe, P. G. Hartley, Unzipping the role of chirality in nanoscale self-assembly of tripeptide hydrogels, Nanoscale 4 (2012) 6752–6760.
[62] S.P. Yeap, J. Lim, H.P. Ngang, B.S. Ooi, A.L. Ahmad, Role of particle–particle interaction towards effective interpretation of Z-average and particle size distributions from dynamic light scattering (DLS) analysis, J. Nanosci. Nanotechnol. 18 (2018) 6957–6964.
[63] S.K. Filippov, R. Khusnutdinov, A. Murmiliuk, W. Inam, L.Y. Zakharova, H. Zhang, V.V. Khutoryanskiy, Dynamic light scattering and transmission electron microscopy in drug delivery: a roadmap for correct characterization of nanoparticles and interpretation of results, Mater. Horiz. 10 (2023) 5354–5370.
[64] X. Yan, Y. Cui, Q. He, K. Wang, J. Li, W. Mu, B. Wang, Z.C. Ou-yang, Reversible transitions between peptide nanotubes and vesicle-like structures including theoretical Modeling studies, Chem. Eur. J. 14 (2008) 5974–5980.
[65] J. Zheng, C. Zhu, X. Xu, X. Wang, J. Fu, Supramolecular assemblies of multifunctional microgels for biomedical applications, J. Mater. Chem. B 11 (2023) 6265–6289.